DOE/JPL-954607-78/1
DISTRIBUTION CATEGORY UC-63

QUARTERLY REPORT NO. 2
DEVELOPMENT AND TESTING
OF
SHINGLE-TYPE SOLAR CELL MODULES

JPL CONTRACT NO. 954607

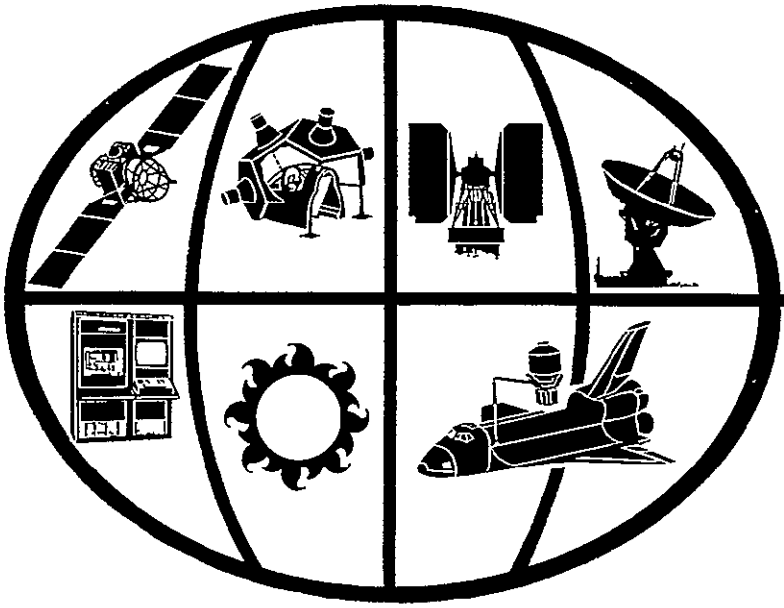

space division

GENERAL ELECTRIC

DOE/JPL-954607-78/1
DISTRIBUTION CATEGORY UC-63

QUARTERLY REPORT NO. 2

DEVELOPMENT AND TESTING
OF
SHINGLE-TYPE SOLAR CELL MODULES

JPL CONTRACT NO. 954607

PREPARED BY: N. F. SHEPARD
REPORT DATE: JANUARY 5, 1978

This work was performed for the Jet Propulsion Laboratory, California Institute of Technology, under NASA Contract NAS7-100 for the U. S. Department of Energy, Division of Solar Energy.

The JPL Low-Cost Silicon Solar Array Project is funded by the DOE and forms part of the DOE Photovoltaic Conversion Program to initiate a major effort toward the development of low-cost solar arrays.

GENERAL ELECTRIC
SPACE DIVISION
Valley Forge Space Center
P O Box 8555 • Philadelphia, Penna 19101

This report contains information prepared by the General Electric Company, Space Division under a JPL subcontract. Its content is not necessarily endorsed by the Jet Propulsion Laboratory, the California Institute of Technology, the National Aeronautics and Space Administration or the Department of Energy.

ABSTRACT

The details of a shingle module design which produces in excess of 97 watts/m^2 of module area at 1 kW/m^2 insolation and at 60° C are reported. This selected design employs a tempered glass coverplate to provide the primary solar cell structural support. The use of the B. F. Goodrich *FLEXSEAL* roofing system as the outer skin of the shingle substrate provides a high confidence of achieving the 15 year service life goal. The fabrication and testing of a preproduction module of this design has demonstrated that this selected approach will meet the environmental testing requirements imposed by the contract.

Attempts to fabricate a preproduction module of an alternative design, which embeds the solar cell assembly within a methyl methacrylate casting, proved unsuccessful.

TABLE OF CONTENTS

LIST OF ILLUSTRATIONS

LIST OF TABLES

SECTION 1
SUMMARY

SECTION 1

SUMMARY

A shingle module, which employs a tempered glass coverplate as the primary solar cell structural support, has been designed and presented for JPL approval. The evolution of this design concept is the result the initial task activities which were completed during the first six months of the contract. Two separate module design concepts were advanced as possible candidate approaches. The first of these involved embedding the interconnected solar cells within a methyl methacrylate (MMA) casting which provided for encapsulation as well as the structural support for the solar cells. The second, and final recommended design, sandwiches the interconnected solar cells between a sheet of tempered low-iron glass on the front surface and a sheet of fiberglass/epoxy on the rear side. The solar cells are bonded to this glass coverplate with polyvinyl butyral (PVB) film and the interstitial space between the covers is filled with RTV 77, which functions as the primary encapsulant.

A set of detail drawings was prepared for each of these design concepts to enable the fabrication of a single preproduction module of each type for evaluation prior to the design review. An attempt to embed a 19-cell assembly, which had been previously buffer coated with RTV615, within a MMA casting proved unsuccessful. This transparent silicone buffer coating, which was applied to elastically accommodate the thermal induced strains at the solar cell/MMA interface, turned cloudy upon the polymerization of the MMA and created an unacceptably large transmission loss. Bulging of the casting at the cell locations was also apparent upon reheating the casting. The volumetric thermal expansion of the RTV615 was evidently sufficient to cause this permanent bulging and associated delamination at the RTV 615/MMA interface.

A preproduction module of the tempered glass covered design was successfully produced as shown in Figure 1-1. During the course of this work several refinements to processing steps were identified to eliminate problems which were experienced during the production of this first module.

This design concept has been approved by JPL for the fabrication of the 50 modules which are deliverable under this contract.

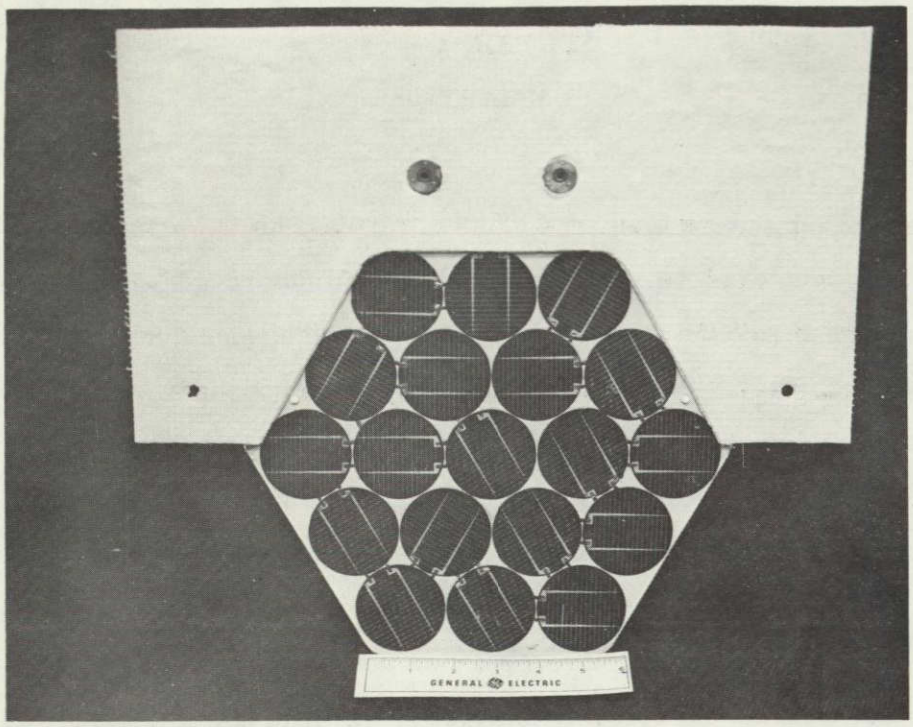

(a) Front (VF Photo No. 77-557B)

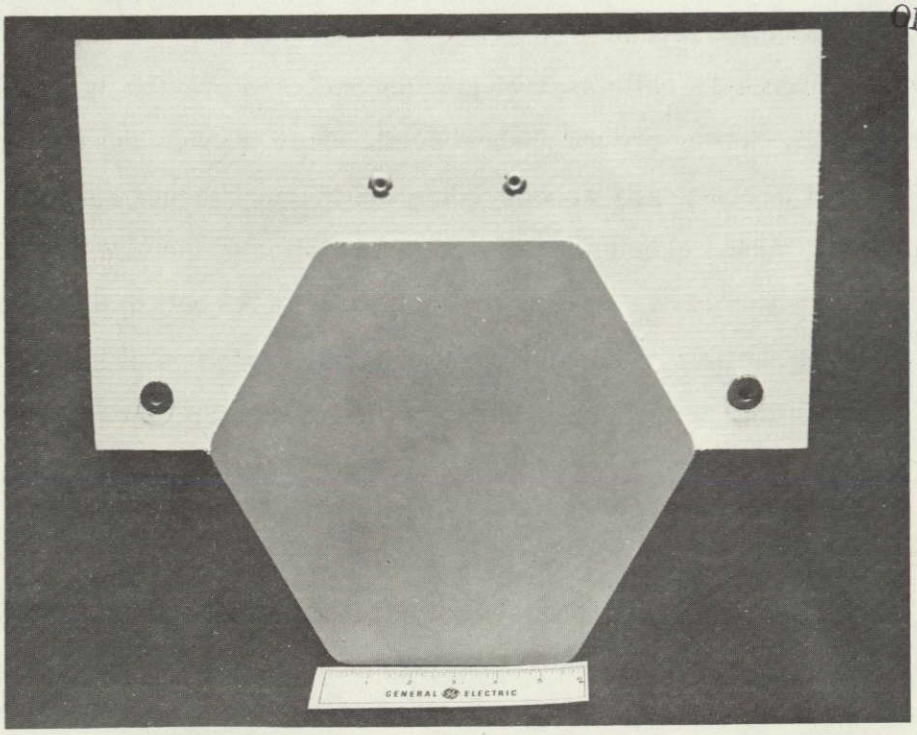

(b) Back (VF Photo No. 77-557A)

Figure 1-1. Tempered Glass Covered Preproduction Module

SECTION 2

INTRODUCTION

SECTION 2

INTRODUCTION

The general scope of work under this contract involves the design, development, fabrication and testing of a solar cell module which is suitable for use in place of shingles on the sloping roof of residential or commercial buildings. Modules of this type employ a semi-flexible substrate which is suitable for mounting on an independent rigid surface such as plywood roof sheathing. As specified in the contract statement of work, these modules shall be capable of producing an electrical power output of 80 W/m^2 of installed module area at a module temperature of 60°C with an insolation of 1 kW/m^2. The installed weight of these shingle-type modules shall not exceed 250 kg/kW of peak power output. As a design goal these modules shall be designed for a service life of at least 15 years. An implicit requirement is that the shingle not sustain damage during the normal handling associated with installation on a roof. The vulnerability to the localized bearing loads associated with walking or kneeling on the installed shingles does not constitute a design requirement but will be assessed as part of this development effort. The program is organized into six major tasks as given below.

Task No.	Description
1	Substrate Evaluation and Testing
2	Solar Cell Tray Evaluation and Testing
3	Module Interconnection and Testing
4	Shingle Module Design
5	Fabrication and Acceptance Testing of Modules
6	Qualification Testing of Modules

The completion of the first four task activities has resulted in the selection of a recommended shingle module design. The details of this design, as described in Section 3.1, were presented to JPL at a design review meeting held on December 16, 1977. JPL approval has been received to proceed with the fabrication and testing of 50 production modules which constitute the deliverable hardware under this contract.

SECTION 3

TECHNICAL DISCUSSION

SECTION 3

TECHNICAL DISCUSSION

3.1 DESCRIPTION OF SELECTED DESIGN

3.1.1 GENERAL DESCRIPTION

The selected design for the shingle solar cell module is represented by the assembly drawing shown in Figure 3-1. This module consists of two basic functional parts: an exposed rigid portion which contains the solar cell assembly, and a flexible portion which is overlapped by the higher courses of the roof installation. The design of the shingle module provides a closely packed array of 19 series – connected solar cells. A minimum separation of 0.5 mm (0.020 inch) is maintained between adjacent cells by assembly tooling which positions the cells prior to bonding to the glass coverplate. The position of the four output terminals of the module has been established to permit the connection of the negative terminals of the next higher course on the roof directly to the positive terminals of the course below. The method of connection, which uses a machine screw and flat washer, will be discussed in Section 3.1.6.

As shown in Sections C-C and D-D of Figure 3-1, the top substrate *FLEXSEAL* skin overlaps, and is bonded to, the glass coverplate to form a weather-tight joint around the upper three sides of the hexagon. The bottom skin and printed wiring board are sandwiched between the glass coverplate and the bottom fiberglass/epoxy cover to produce a similar seal around these three edges on the bottom.

The key features of this selected design are summarized in Table 3-1. The calculated module output of 4.9 Watts at 1 kW/m^2 and 60° C yields a specific output of 97 $Watt/m^2$ of module area. This is 21 percent better than the minimum requirement of the contract. The specific weight of the module is 204 kg/kW of peak power output at kW/m^2 and 60° C as compared to a maximum specified value of 250 kg/kW.

Table 3-1. Key Features of Selected Module Design

Parameter	Value
Total Solar Cell Area	419.2 cm^2
Module Area	507.0 cm^2
Packing Factor	0.827
Electrical Power Output at the Maximum Power Point (Minimum Average)	
AM1, 1 kW/m^2 and 28°C	5.8 Watts
AM1, 1 kW/m^2 and 60°C	4.9 Watts
Module Weight	1.00 kg

3.1.2 SUBSTRATE CONFIGURATION

The flexible substrate portion of the shingle is of laminar construction as shown in Figure 3-2. The two outer-skins of this substrate are *FLEXSEAL* polyester scrim reinforced *HYPALON*. This material is white in color and provides the weather-resistance properties required to meet the 15 year service life goals. A center core of closed cell epichlorohydrin foam (Rubatex No. R-473-E) provides a low-density, high-temperature resistant filler material to achieve a nearly uniform thickness of the entire surface area of the shingle. The substrate also affords protection to the flexible printed wiring board which is sandwiched between the bottom skin and the core. This double sided printed wiring board, which carries both the positive and negative terminations for the module, is shown in Figure 3-3. The raw material is identified by GE designation FLGF .006 C 2/2 and consists of 2 oz/ft^2 copper foil on both sides of a .006 inch thick fiberglass/epoxy substrate. This copper is etched away to form the bus strip patterns shown in the figure. The calculated series resistance of this copper bus network is the 4.6 mΩ at 20°C, which represents a negligible power loss.

The entire composite substrate is bonded together with the B. F. Goodrich adhesive system described in Table 3-2. This contact adhesive and associated primers are traditionally used as part of the *FLEXSEAL* roofing system. Two different primers have been specified depending upon the nature of the surface to be bonded. In either case the primer is applied in a very

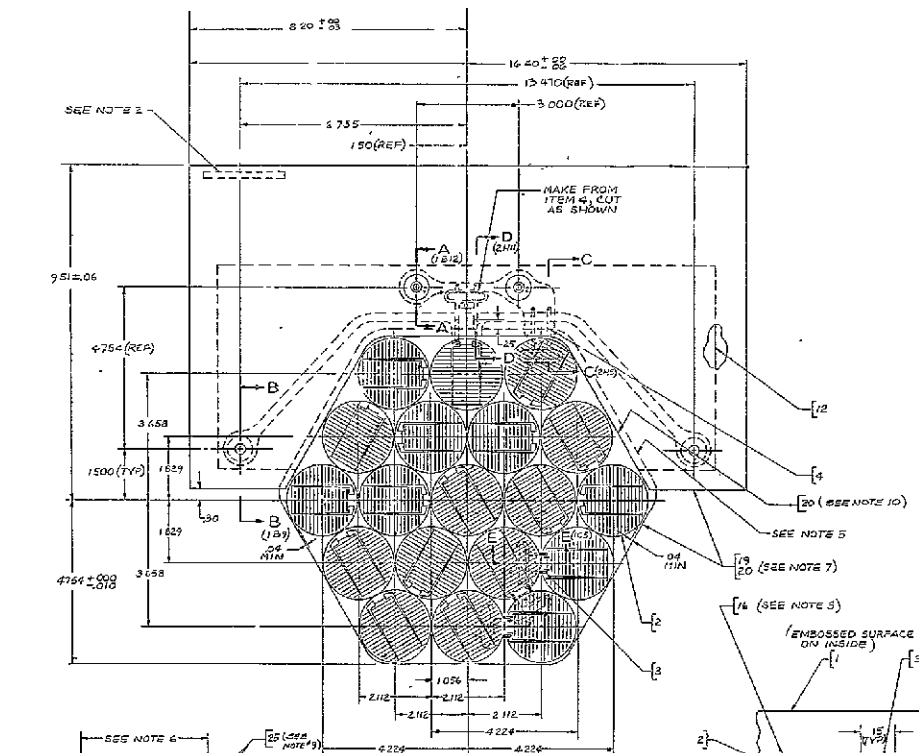

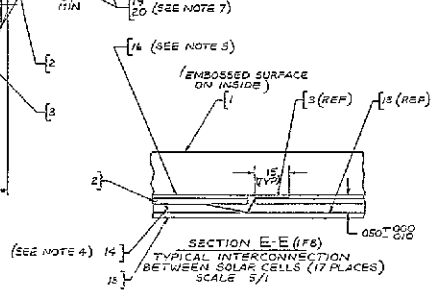

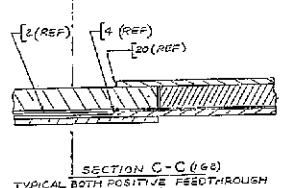

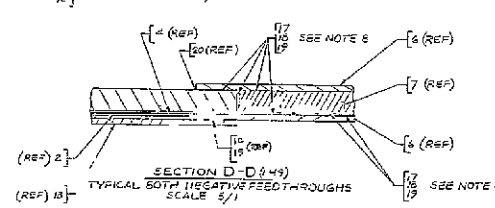

NOTES

1. INTERPRETATION OF DRAWING TERMS AND TOLERANCES PER SS-S-00009
2. MARK PART "2399-4782327796-" AS APPLICABLE PER 1184152626 CL 21E
3. HEAT SEAL SOLAR CELLS (ITEM 2) TO EMBOSSED SURFACE OF GLASS COVERPLATE (ITEM 1) USING ITEM 16. THE ENTIRE CELL SURFACE MUST BE BONDED TO THE GLASS. ITEM 16 SHALL NOT PROJECT MORE THAN .010 RADIUS BEYOND THE CELL CIRCUMFERENCE
4. FILL VOID BETWEEN ITEMS 1 AND 18 WITH ITEM 14. PRIME SURFACES OF ITEMS 1, 6 AND 18 WITH ITEM 15. AFTER CURING, TRIM ITEM 14 AROUND EDGES OF GLASS COVERPLATE
5. CUT ITEM 7 TO MATCH GLASS COVERPLATE (ITEM 1) AT FINAL ASSEMBLY
6. CUT HOLES IN ITEM 6 TO MATCH CORRESPONDING DIAMETERS OF ITEMS 8 AND 9
7. FOLLOWING FINAL TRIMMING OF OVERALL DIMENSIONS, COAT EXTERIOR EDGES OF SUBSTRATE AND GLASS COVERPLATE WITH ITEMS 19 AND 20. (REFER TO PIR 1R30-528 FOR BONDING INSTRUCTIONS)
8. BOND ITEMS 1 TO 6, 2 TO 1, 5 TO 7, 7 TO 1, 21 TO 23, 22 TO 24, 12 TO 6, AND 12 TO 7 USING ITEM 19. PRIME SURFACES OF ITEMS 5, 12, WITH ITEM 17 AND SURFACE OF ITEMS 6, 7, 21, 22, 23 AND 24 WITH ITEM 18. (REFER TO PIR 1R30-528 FOR BONDING INSTRUCTIONS).
9. BOND ITEMS 8 TO 10, AND 16 TO 11 USING ITEM 25.
10. RUN A FILLET OF ITEM 20 ALONG THE INTERFACE BETWEEN ITEMS 1 AND 6.

Figure 3-1. Tempered Glass Covered Module Design

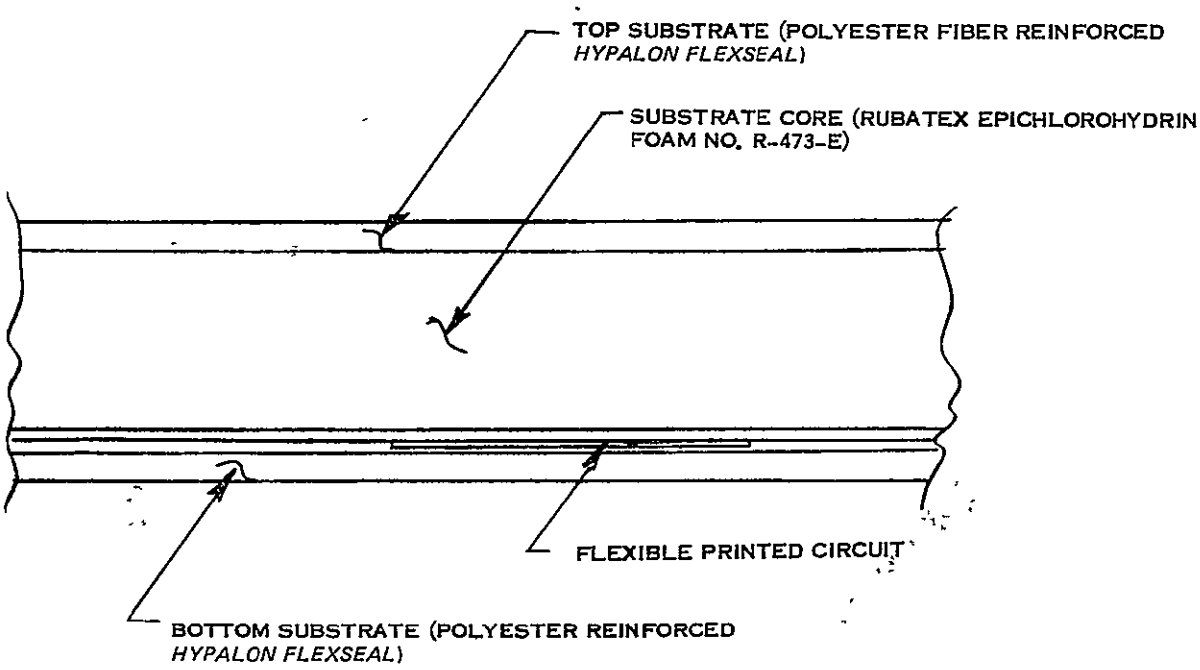

Figure 3-2. Section Through Shingle Module Substrate

Table 3-2. Substrate Adhesive System

Identification No.*	Description/Application
A 1104-B	Primer for Non-porous Surfaces (e.g., glass)
A 178-B	Primer for Porous Surfaces (e.g., foam)
CA-1056	Contact Adhesive (all surfaces)
A 1436-B	Edge Sealer

* B. F. Goodrich Co.
General Products Division
Solon, Ohio 44139

thin coating and allowed to dry thoroughly prior to the application of the contact adhesive to both surfaces to be bonded. The contact adhesive film is allowed to dry to a tack-free state prior to contacting the two surfaces to be joined. The edge sealer (A1436-B) is applied to the outer edges of the substrate to seal the exposed foam core material.

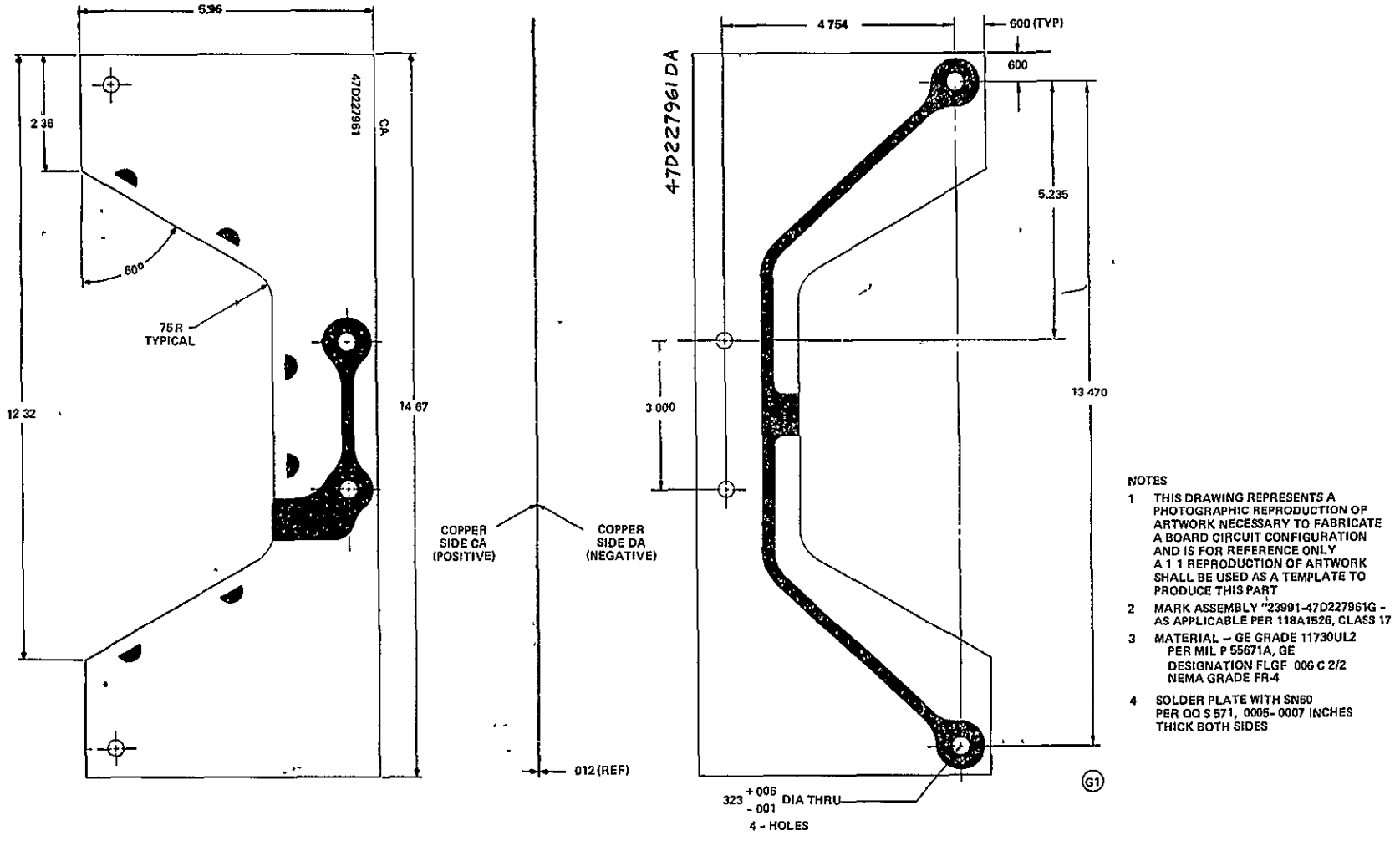

NOTES

1. THIS DRAWING REPRESENTS A PHOTOGRAPHIC REPRODUCTION OF ARTWORK NECESSARY TO FABRICATE A BOARD CIRCUIT CONFIGURATION AND IS FOR REFERENCE ONLY. A 1 1 REPRODUCTION OF ARTWORK SHALL BE USED AS A TEMPLATE TO PRODUCE THIS PART
2. MARK ASSEMBLY "23991-47D227961G - AS APPLICABLE PER 118A1526, CLASS 17
3. MATERIAL -- GE GRADE 11730UL2 PER MIL P 55671A, GE DESIGNATION FLGF 006 C 2/2 NEMA GRADE FR-4
4. SOLDER PLATE WITH SN60 PER QQ S 571, 0005- 0007 INCHES THICK BOTH SIDES

Figure 3-3. Substrate Printed Wiring Board Design

A load-deflection test was performed on a segment of the substrate consisting of a top and bottom skin of polyester scrim reinforced *FLEXSEAL* bonded to a core of epichlorohydrin foam. The resulting load-deflection curve with a 14.3 mm (0.563 inch) diameter bearing surface is as given in Figure 3-4. The use of these data in the determination of module-to-module interconnection joint contact force will be discussed later.

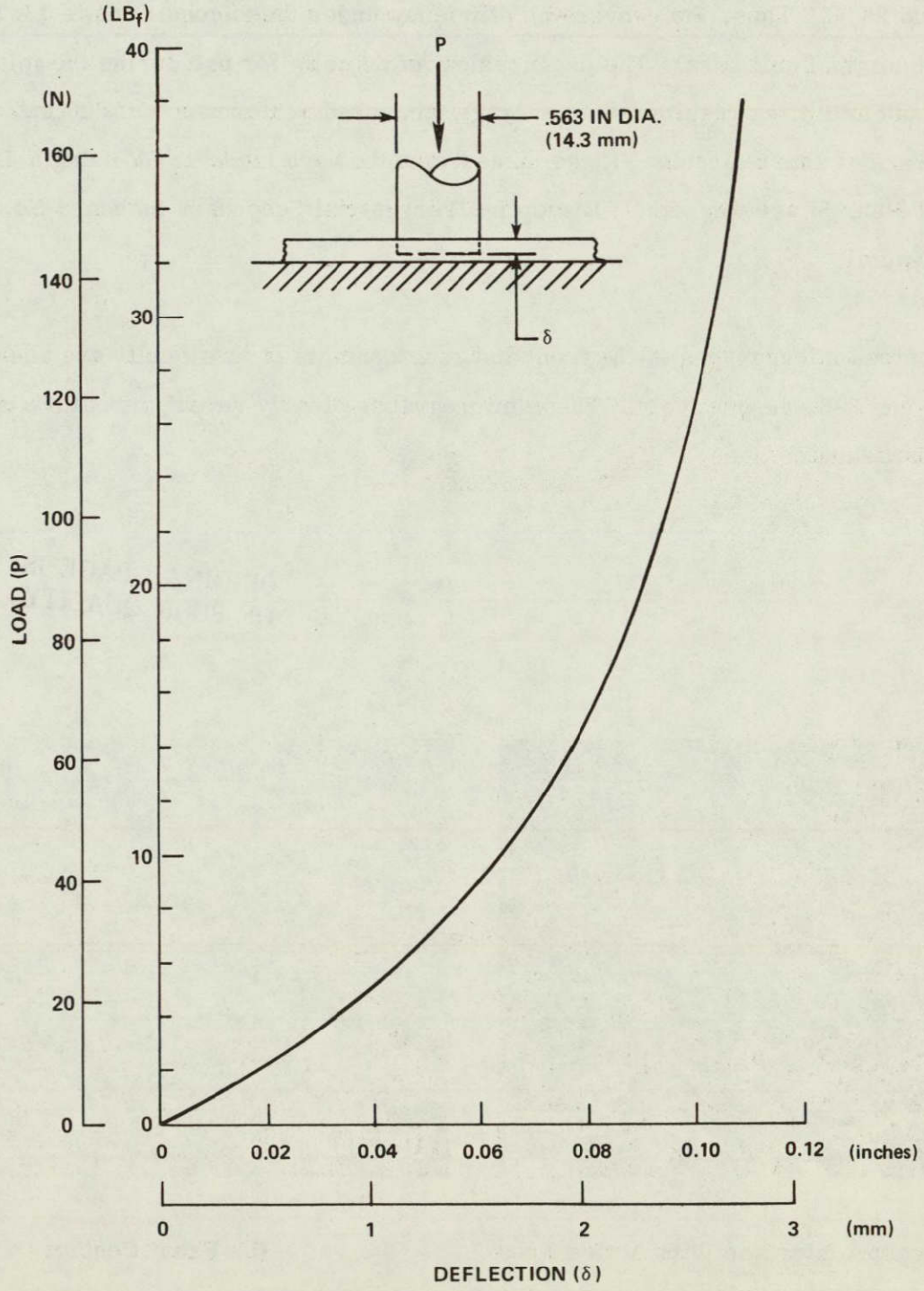

Figure 3-4. Local Bearing Load-Deflection Curve for Substrate

3.1.3 SOLAR CELL SELECTION

A Spectrolab solar cell was selected for use in this module design on the basis of the lowest specific cost of the delivered power output. This cell is specified to have a diameter of $53 \frac{+0.13}{-0.37}$ mm and a minimum electrical power output of 610 mA at 0.475 Volts at 1 kW/m^2 insolation and 28° C. Thus, the conversion efficiency under these conditions is 13.13 percent based on the nominal cell area. The procurement of 50 cells for use during the initial pre-production task activities resulted in an average measured performance of 620 mA at 0.475 Volts and 676 mA at short-circuit. These measurements were made at GE using a Large Area Pulsed Solar Simulator with JPL supplied Terrestrial Secondary Standard No. 025 as the reference cell.

Scanning electron micrographs of the front and rear contacts of these cells are shown in Figures 3-5 and 3-6, respectively. These micrographs clearly reveal the nature of the printed contact surface.

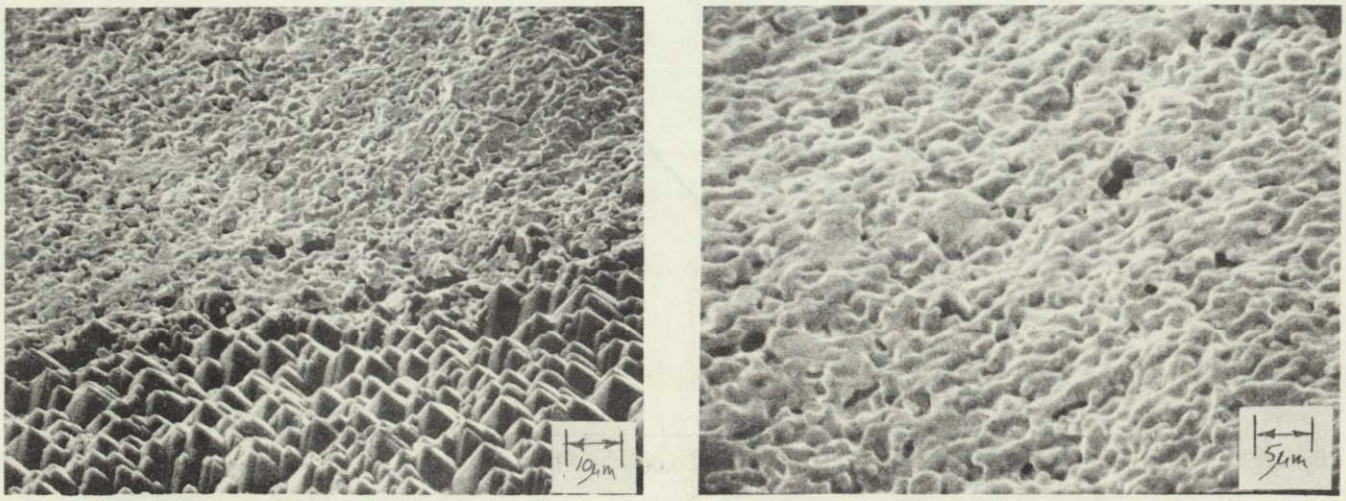

(a) Front Contact Interface With Active Area (b) Front Contact

Figure 3-5. Scanning Electron Micrographs of Solar Cell Front Contact

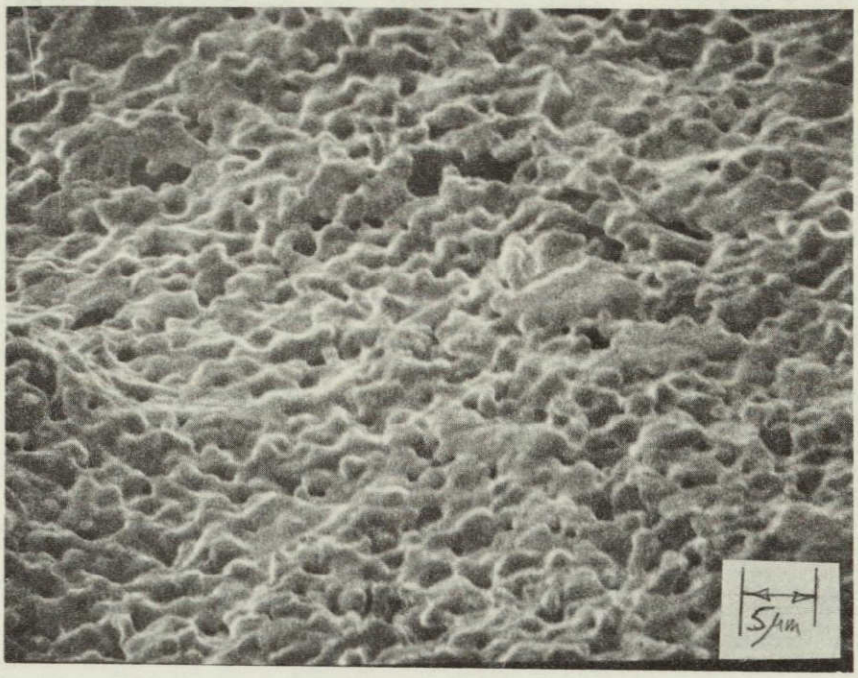

Figure 3-6. Scanning Electron Micrograph of Solar Cell Back Contact

3.1.4 SOLAR CELL INTERCONNECTOR

The solar cell interconnector shown in Figure 3-7 is fabricated from nominal 50 μm (.002 inch) thick soft copper foil (Alloy No. 110) which is subsequently solder plated to a thickness of 13 to 18 μm (.0005 to .0007 inch) on both surfaces. The resistance of this interconnector measured between the two "N" joints and the three "P" joints is 1.67 mΩ at 25°C. At 60°C this series resistance loss amounts to 0.3 percent of the cell maximum power output. Figure 3-8 shows a typical "N" contact solder-joint which was made by reflowing the solder plating on the interconnector with a hand soldering iron.

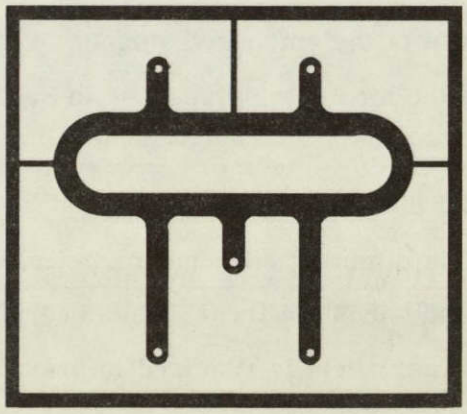

Figure 3-7. Solar Cell Interconnector

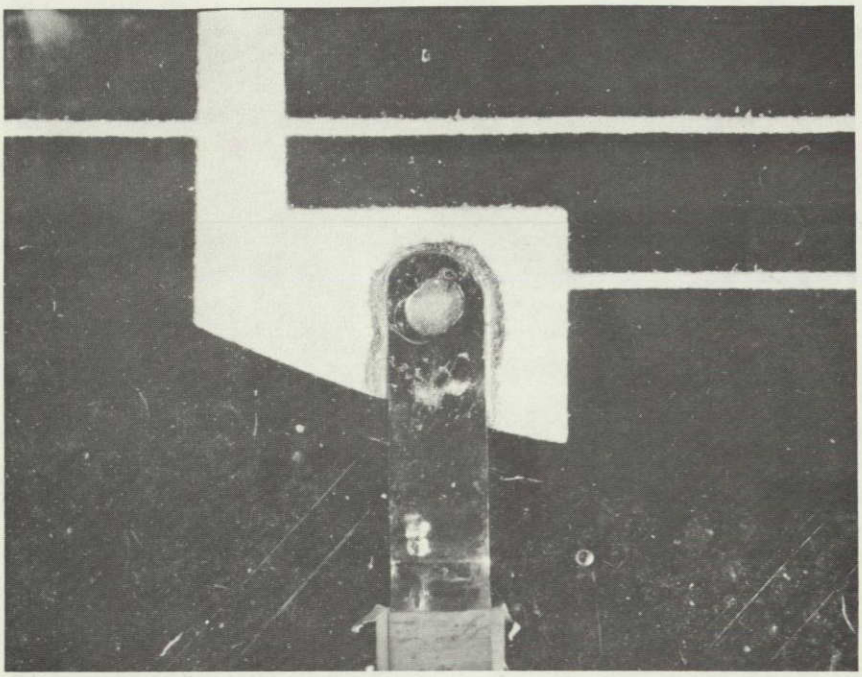

Figure 3-8. Typical "N" Contact Solder Joint

3.1.5 MODULE ENCAPSULATION

The details of the encapsulation surrounding the solar cell assembly are shown in Figure 3-9. The solar cells are individually bonded to the underside of the glass coverplate with disks of Monsanto *SAFLEX* PT-10 PVB film. This glass coverplate is fabricated from ASG *SUNADEX* low-iron glass (0.01% iron-oxide content) which is cut to the shape shown for the P1 part in Figure 3-10 and then thermally tempered to provide the flexural strength required to sustain the bearing loads associated with walking or kneeling. The transmission of this glass is compared with that of ASG *LO-IRON* (0.05% iron-oxide content) in Figure 3-11. These data do not indicate a clear transmittance advantage associated with the use of the *SUNADEX* glass, but this selecton was made because of the embossed surface texture of this glass and its influence on the enhanced output of the module as discussed in Section 6.

The primary encapsulation around the solar cells is provided by RTV 77, which is a white spreadable thixotropic paste. This dimethyl silicone compound fills the space surrounding the solar cells and interconnectors and bonds the front glass coverplate to the rear protective sheet of fiberglass/epoxy. This rear sheet is required to prevent damage to the module from sharp objects such as nails which are ever-present during the installation of a shingle roof.

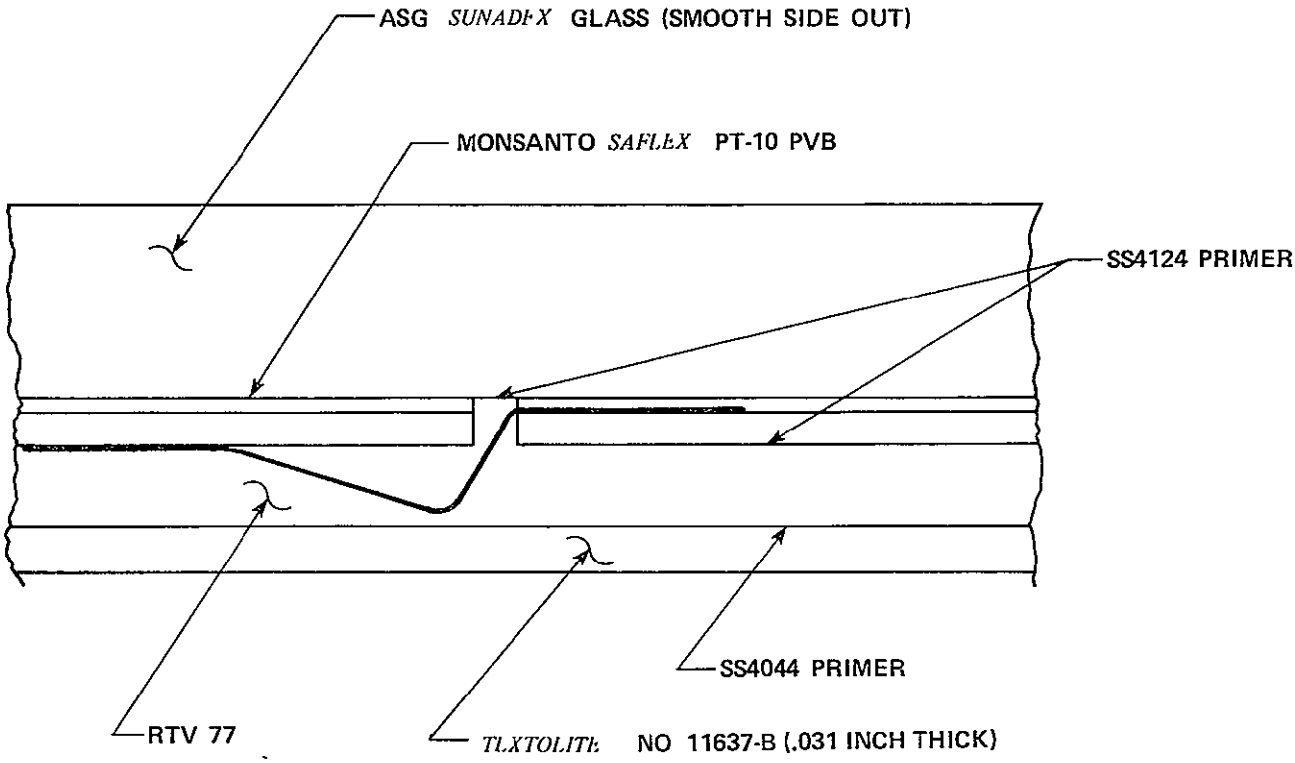

Figure 3-9. Module Encapsulation

3.1.6 MODULE-TO-MODULE INTERCONNECTION

The module-to-module interconnection is accomplished as shown in Figure 3-12. This basic concept relies on the development of high contact pressure under three conical projections, which are part of solder plated copper bosses within each mating shingle, to achieve a low-resistance, environmental stable connection. The development activity which led to the selection of this approach is discussed in Section 3.3.

The two positive terminals of each shingle are provided with these copper bosses which are soldered to the circular pads on the top of the printed circuit board, as shown in Section A-A of Figure 3-1. A 6-32 *TEENUT*, which has been modified by shortening the barrel and removing the prongs, is centered within each of these positive terminals with an insulating sleeve. Both this sleeve and the *TEENUT* are made captive by bonding to each other and to the copper boss. The *TEENUT* is thus insulated from the positive terminal by the sleeve and by the bottom *FLEXSEAL* skin under the circuit board. The two negative terminals of each module are provided with thinner copper bosses which are soldered to the bottom of the printed circuit board at the circular pad mounting locations. Upon assembly, contact pressure is developed between these two overlapping copper bosses by compressing the substrate core

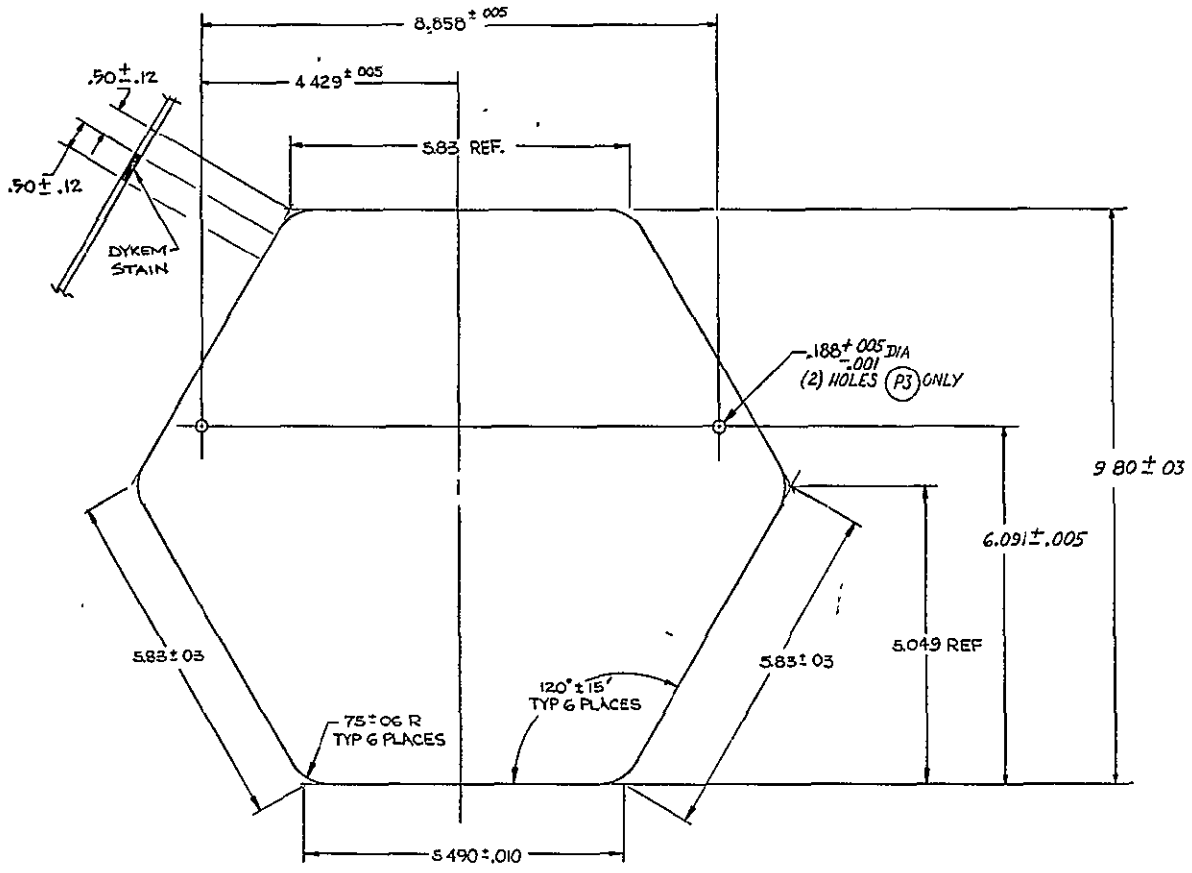

NOTES

1. DRAWING TERMS & TOLERANCES PER S30009
2. THE MEAN MODULUS OF RUPTURE IN BENDING SHALL EXCEED (LATER) PSI WHEN TESTED IN ACCORDANCE WITH METHOD A OF ASTM C158-72 "FLEXURE TESTING OF GLASS

(P1) THERMALLY TEMPERED ASG SUNADEX GLASS 125 ± 005 THK

(P4) SAME AS P1 EXCEPT MATERIAL IS TEXTOLITE NO 11637-B, .031 THK (STK)

(P2) CHEMICALLY STRENGTHENED LOW-IRON SODA-LIME GLASS .085 ± 005 THICKNESS

(P3) "SAME AS (P1) EXCEPT AS NOTED

Figure 3-10. Coverplate Design

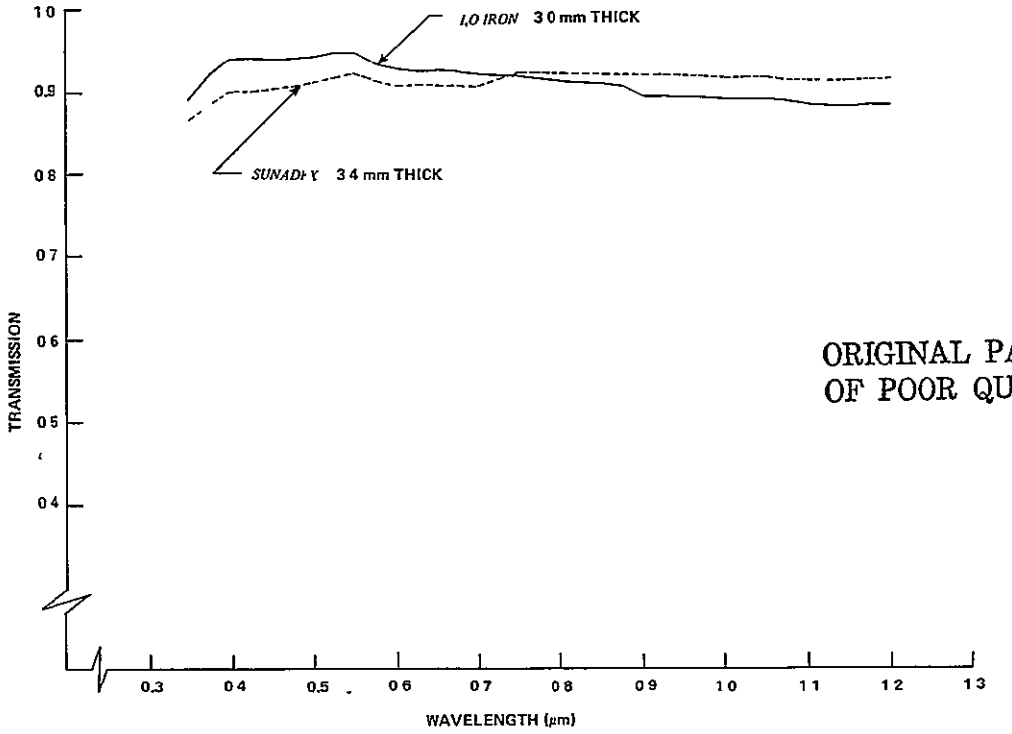

Figure 3-11. Transmission of ASG Low-Iron Soda-Lime Glasses Without Anti-Reflection Coating

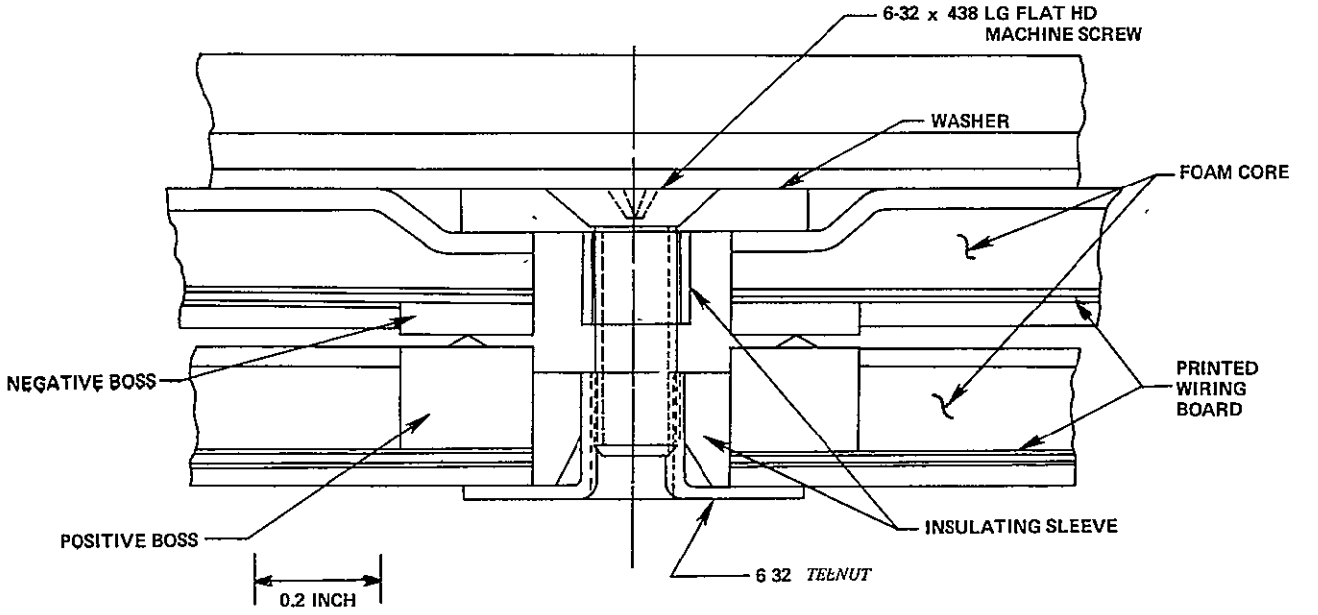

Figure 3-12. Module-to-Module Interconnection

with a 6-32 flat head machine screw and 14.3 mm (0.563 inch) diameter flat washer. The screw is driven into the *TEENUT* until the top surface of the washer is flush with the top surface of the outer *FLEXSEAL* skin. Under these conditions the 1.8 mm (0.070 inch) thick washer will have developed a total compressive force of 52 N (see Figure 3-4) or 17.3 N per conical projection. As reported in Section 3.3, this is adequate force to provide a reliable high-pressure, gas-tight contact. The insulating sleeve around the screw thread prevents electrical contact with the negative terminal of the module so that the exposed screw head/ washer/ *TEENUT* are electrically neutral after installation. This interconnector design concept is also capable of accommodating up to 1.8 mm (0.07 inch) of misregistration between centerlines.

3.1.7 ELECTRICAL PERFORMANCE ANALYSIS

The prediction of module electrical performance is based on the expected average output of the bare solar cells. As mentioned in Section 3.1.3, the initial 50 solar cells procured from Spectrolab under this contract yielded the following average bare cell performance:

$$I_{SC} = 676 \text{ mA}$$

$$I_{0.475V} = 620 \text{ mA}$$

$$V_{OC} = 0.580 \text{ Volt}$$

These values are considered representative of the expected average performance for the larger quantity required for the production modules. These average bare cell performance parameters were modified to account for the effects of encapsulation by applying the following intensity modification factors to the average bare cell short-circuit current:

Factor	Value
Net Transmittance Loss in Glass Coverplate and PVB Film	0.98
Enhancement in Module Output Due to Reflection from White Interstitial Spaces	1.06
Net Effect on Module I_{SC}	1.039

The first of these factors accounts for the estimated transmittance loss in the *SUNADEX* glass and in the PVB film as well as the reflection loss at the air/glass interface with no anti-reflective (AR) coating on the outer glass surface. A value of 0.98 is estimated for the net effect of these transmittance losses since these negative factors are nearly compensated for by the improved optical coupling between the cell AR coating and the PVB film. The second factor represents the measured enhancement in cell short-circuit current as a result of the capture of the reflected light from the white interstitial spaces as described in Section 6. For the selected shingle design, Figure 3-13 shows the relative short-circuit current as a function of packing factor. With an overall packing factor of 0.827, these data indicate an expected enhancement of 6 percent due to this phenomena. The temperature-dependence of the basic solar cell performance parameters as given in Table 3-3 were used, along with the calculated series resistance of the interconnectors and termination bus strips, in the calculation of the I-V characteristics given in Figure 3-14. The expected minimum average module electrical output is calculated to be 4.9 watts at a 7.7 volt maximum power voltage at 1 kW/m^2 and 60^{o}C.

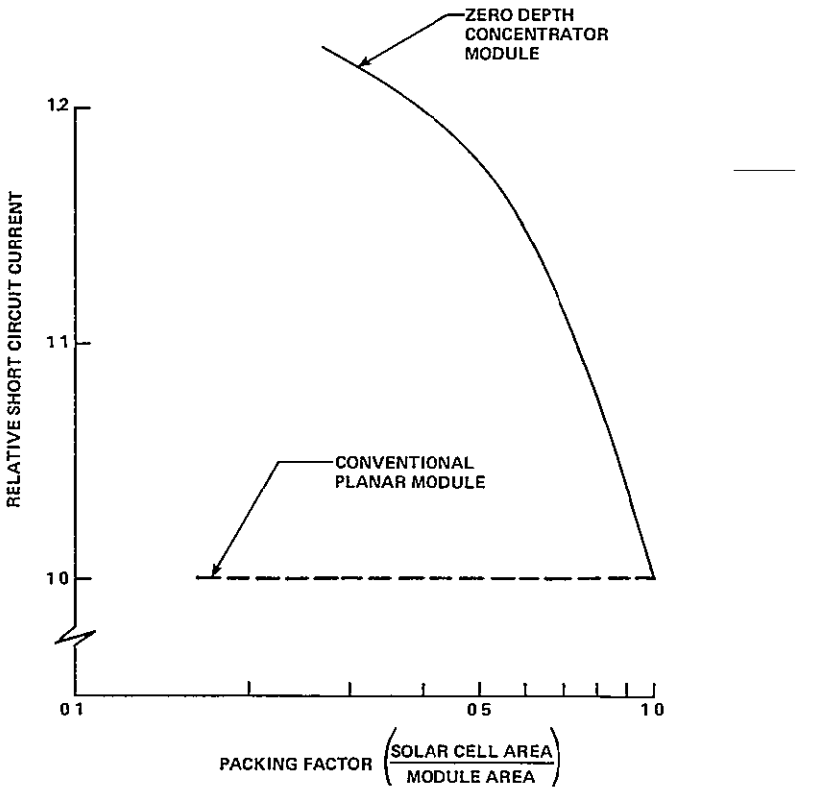

Figure 3-13. Enhanced Module Output With an Embossed Glass Coverplate and White Interstitial Spaces

Table 3-3. Temperature Dependence of Solar Cell Performance Parameters

Parameter	Value
$\frac{1}{(I_{sc})_{28C}} \frac{\partial I_{sc}}{\partial T}$	+0.000647
$\frac{1}{(V_{oc})_{28C}} \frac{\partial V_{oc}}{\partial T}$	-0.00352
$\frac{1}{(V_{mp})_{28C}} \frac{\partial V_{mp}}{\partial T}$	-0.00442
$\frac{1}{(P_{max})_{28C}} \frac{\partial P_{max}}{\partial T}$	-0.00462

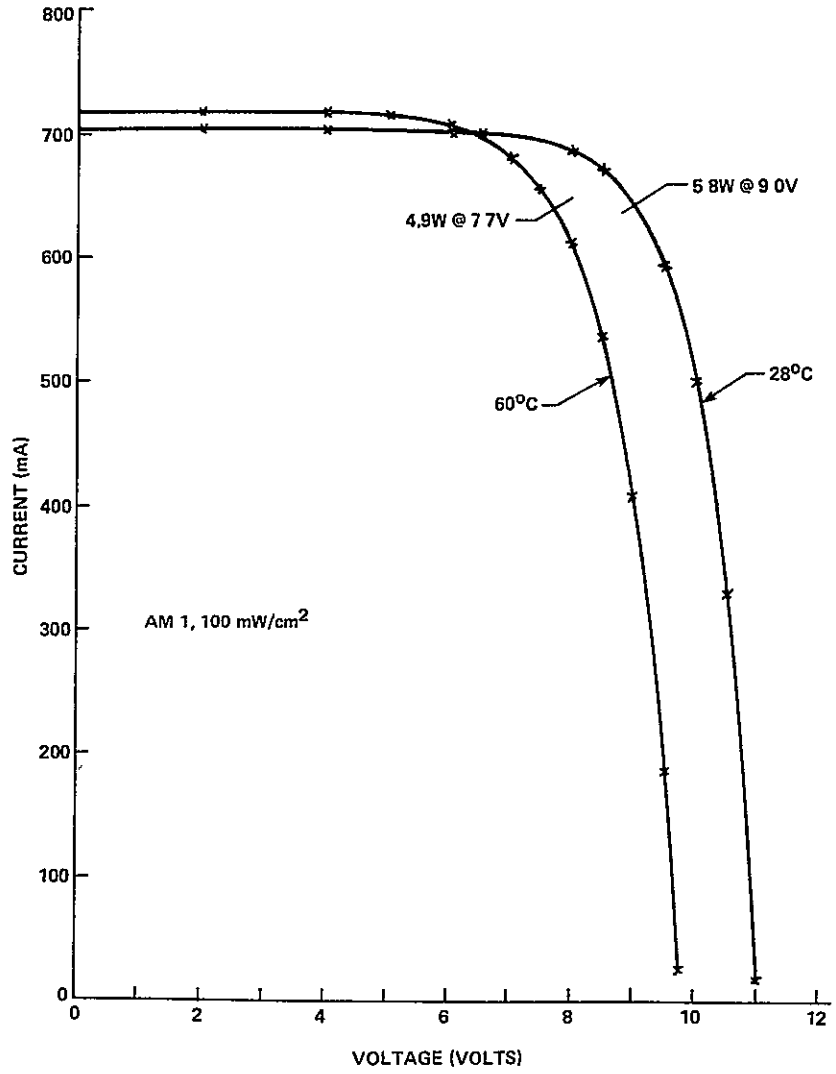

Figure 3-14. Expected Minimum Average Module Electrical Performance

3.2 PREPRODUCTION MODULE FABRICATION AND TESTING EXPERIENCE

3.2.1 METHYL METHACRYLATE MODULE

Single cell test specimens have been successfully embedded within methyl methacrylate (MMA) castings, but subsequent thermal cycle testing of these specimens has resulted in the delamination of the cell from the casting and the fracture of the cell and casting as shown in Figure 3-15. Failures of this type, which are related to the low temperature extreme of -40° C, have been experienced on three separate specimens - one of which was tested by JPL. In all cases the MMA has cracked and separated around the circumference of the cell with delamination occurring between the cell and the casting. Fracture of the silicon crystal also occurred in a plane parallel to the active surface. These failures indicate the presence of extremely high stresses as a result of the differential thermal contraction of the two materials. Figure 3-16 shows the relative linear thermal expansion data for these two materials. Since the polymerization of the MMA occurs at approximately 100° C, it could be assumed that the cell and casting were bonded together under a zero stress condition at this temperature. Subsequent cooling to room temperature and to the -40° C low temperature thermal cycling extreme results in a shrinkage of the MMA relative to the solar cell. Using the data from Figure 3-16, this 140° C temperature difference would result in a strain of approximately 1 percent when the temperature is -40° C. The test results indicate that this strain can not be accommodated without the fracture of both materials.

In view of these results it was felt that a transparent buffer coating of a silicone pottant would provide the elastic flexability necessary to accommodate this thermally induced strain. The decision was made to attempt this approach for the 19-cell casting assembly for the MMA preproduction module. Each solar cell was coated front and back with a layer of RTV 615. Following the cure of this buffer coating, the complete interconnected assembly was embedded within a MMA casting. The MMA was successfully polymerized but a reaction between the MMA and the silicone turned the initially transparent buffer coat cloudy. This cloudiness of the RTV 615 virtually obscured the solar cells and resulted in a measured electrical output which was significantly lower than expected. In addition an attempt to anneal the casting by heating to 107° C for four hours resulted in the development of bulges in the casting at each of the 19-cell locations due to the distortion of the MMA under the influences of the volumetric thermal expansion of the RTV 615. The subsequent coating of the casting left permanent

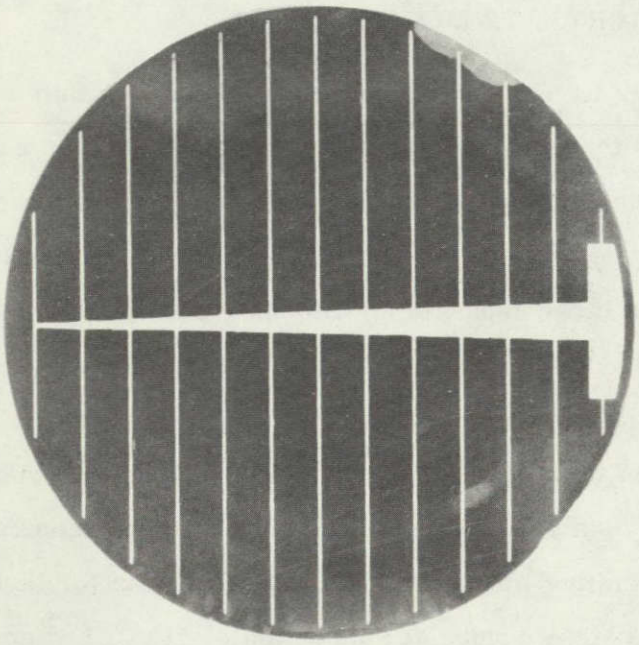

(a) As Fabricated Condition

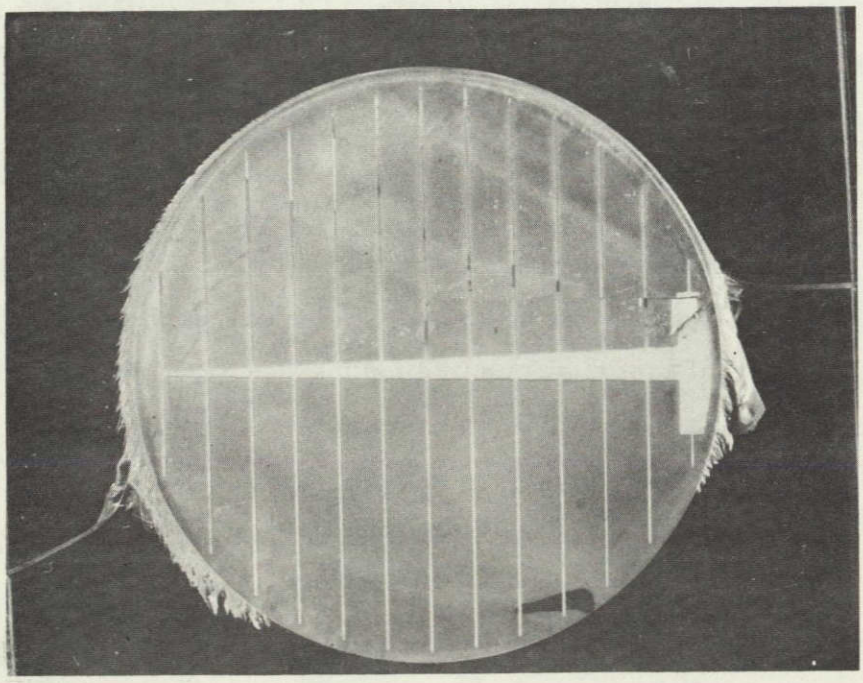

(b) After One Cycle to -40° C

Figure 3-15. Methyl Methacrylate Embedded Single Cell Test Specimen

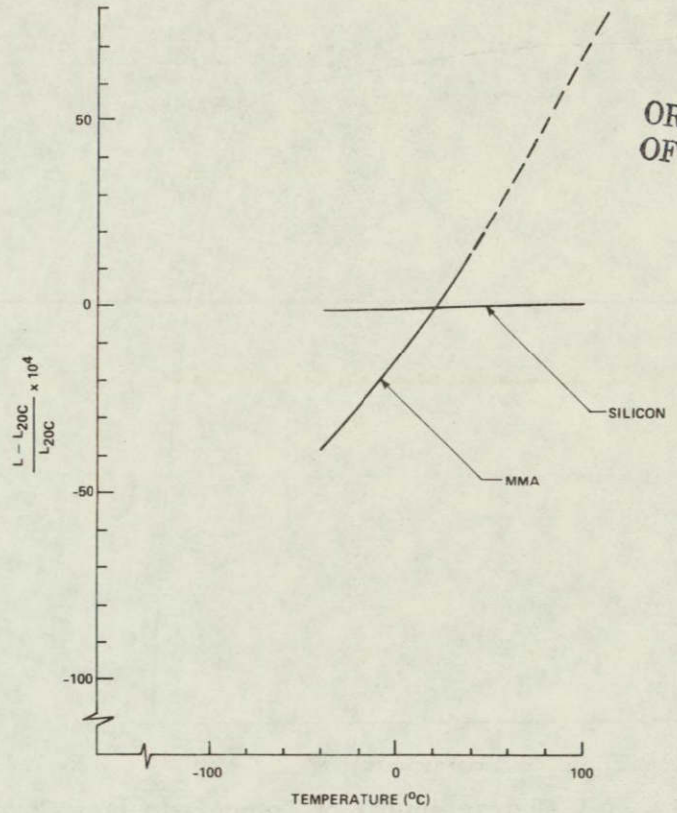

Figure 3-16. Linear Thermal Expansion of Silicon and Methyl Methacrylate

bulges at these cell locations with an associated delamination of the RTV 615 from the MMA. In view of this unsuccessful attempt to produce a casting for the MMA module design, the plan to incorporate this casting into a complete preproduction shingle of this design was discontinued.

3.2.2 TEMPERED GLASS COVERED MODULE

The preproduction shingle module of the tempered glass covered design was completed as shown in Figure 1-1. An illumination test of this completed module yielded the results shown in Figure 3-17. A maximum power point output of 5.9 Watts at 9.25 Volts was measured at 1 kW/m^2 and 28° C using TTS 025 as the reference standard cell. The matching of cells within this module was not ideal due to the short supply of cells with the required output. Consequently, the highest and lowest performance cells in this module had measured bare cell short-circuit currents of 673 and 655 mA and currents at 0.475 Volts of 623 and 570 mA, respectively. The slope of the I-V characteristic in the constant current region reflects this

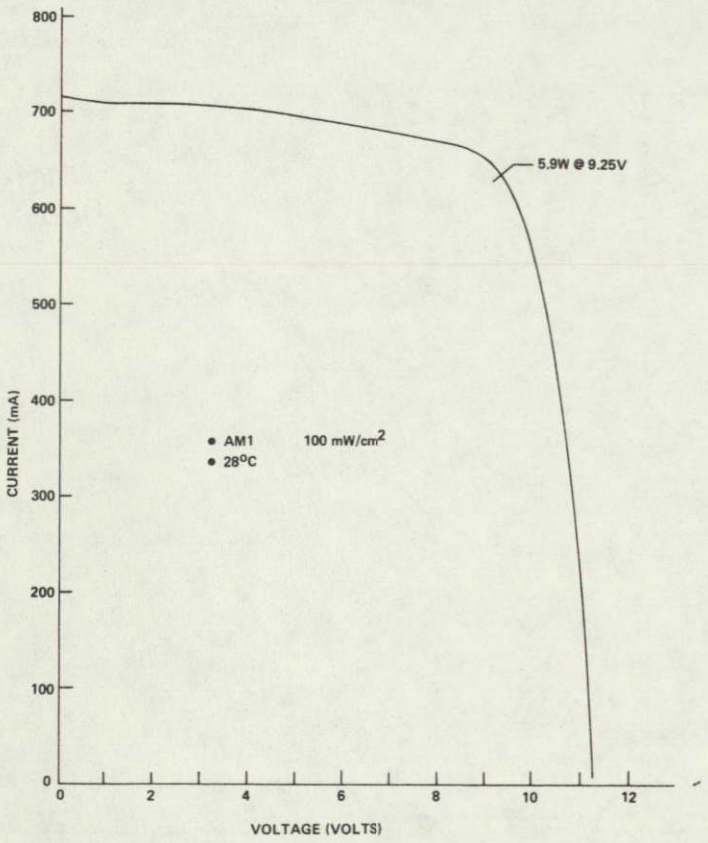

Figure 3-17. I-V Characteristic of Tempered Glass Covered Preproduction Module

large range in individual cell short-circuit current and illustrates a relatively weak reverse voltage breakdown characteristic for the lower performance cells of the group. The module maximum power output exhibits the enhancement in module output resulting from the phenomena reported in Section 6.

During the fabrication of this tempered glass covered preproduction module an excessive amount of air bubbles were trapped within the PVB film. This lamination process involved the application of static pressure to the glass coverplate while the solar cell assembly was held in a bonding fixture which was heated to approximately 165° C (329° F). The elimination of these bubbles within the PBV was achieved on another trial coverplate by the application of vacuum to the space between the coverplate and the bonding fixture by sealing to the bonding fixture around the perimeter of the coverplate with high temperature tape. The atmospheric pressure on the coverplate surface was sufficient to provide bubble-free lamination in the presence of vacuum.

The entrapment of air bubbles between the *FLEXSEAL* skin and the foam core material was also apparent on this preproduction module. The contact adhesive system used to bond these two surfaces is extremely sensitive to the method used to make the initial contact between the surfaces. Contact must be made from one edge of the materials and gradually rolled along a line so that no air pockets are entrapped between the mating surfaces.

The completed preproduction module was subjected to a thermal cycling test between the extremes of -40 to 90° C. Sixteen cycles were completed before a malfunction in the chamber control system caused a high temperature runaway condition. This overtemperature exposure caused the PVB film adhesive between the glass coverplate and cells to bubble. Observations made prior to this malfunction indicated that the small entrapped air pockets between the *FLEXSEAL* skin and the foam core had become more pronounced as a result of the high temperature exposure. Delamination between the RTV 77 and the glass coverplate was also observed to have occurred in the areas between the solar cells, but not at the outer edges of the coverplate. It is postulated that air pockets trapped between the interconnector loops and the glass surface expanded when heated and caused a delamination in these areas. This problem will be eliminated on subsequent modules by deaerating the RTV 77 after it is spread over the glass coverplate. The adhesion of the RTV 77 to the glass coverplate should also be improved by using SS4124 primer on these surfaces instead of SS4044.

The single cell test specimen shown in Figure 3-18, which was fabricated using the same materials as the preproduction module, was subjected to 30 thermal cycles between -40 and 90° C with no measurable change in physical appearance or in electrical output.

3.3 MODULE-TO-MODULE INTERCONNECTION EVALUATION

The three module-to-module interconnector designs shown in Figure 3-19, 3-20, and 3-21 were assembled into simulated shingles, joined together and mounted onto a test specimen as shown in Figure 3-22. This simulated roof section was subjected to a test program which consisted of a random vibration exposure, a thermal cycling test, and a humidity exposure followed by a final random vibration exposure. The test specimen was instrumented as shown in Figure 3-23 to provide a continuous current through each circuit under test and a record of the voltage drop across each circuit.

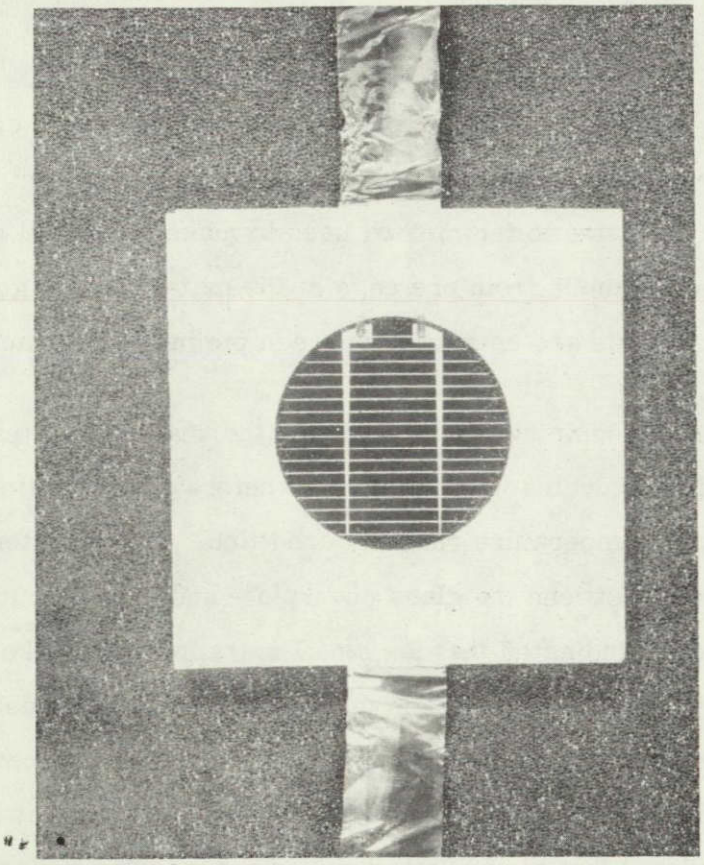

Figure 3-18. *SUNADEX* Glass Covered Test Specimen

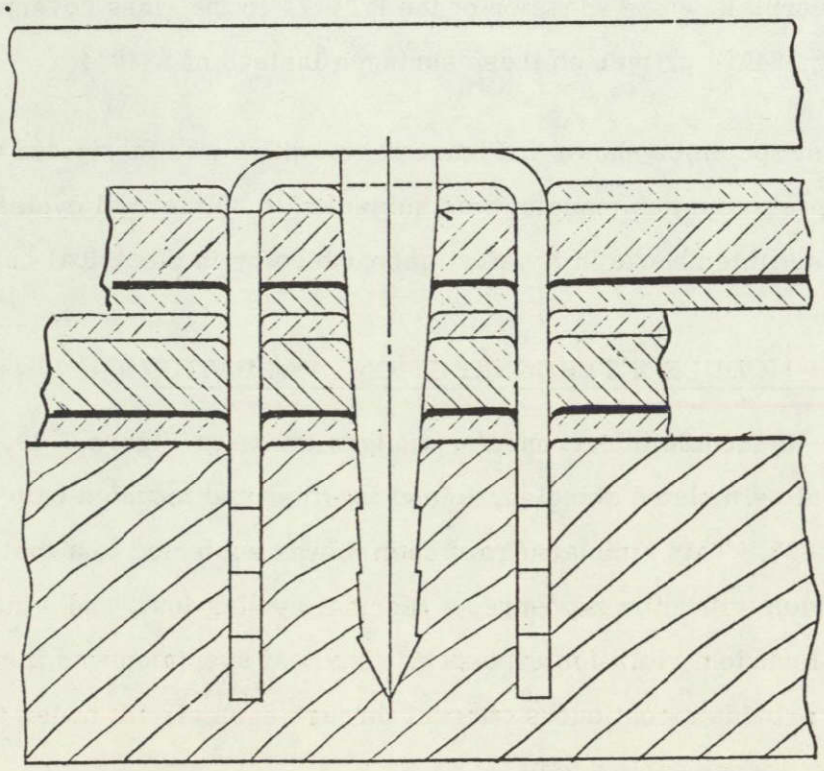

Figure 3-19. Four-Pronged Nail Module Interconnector

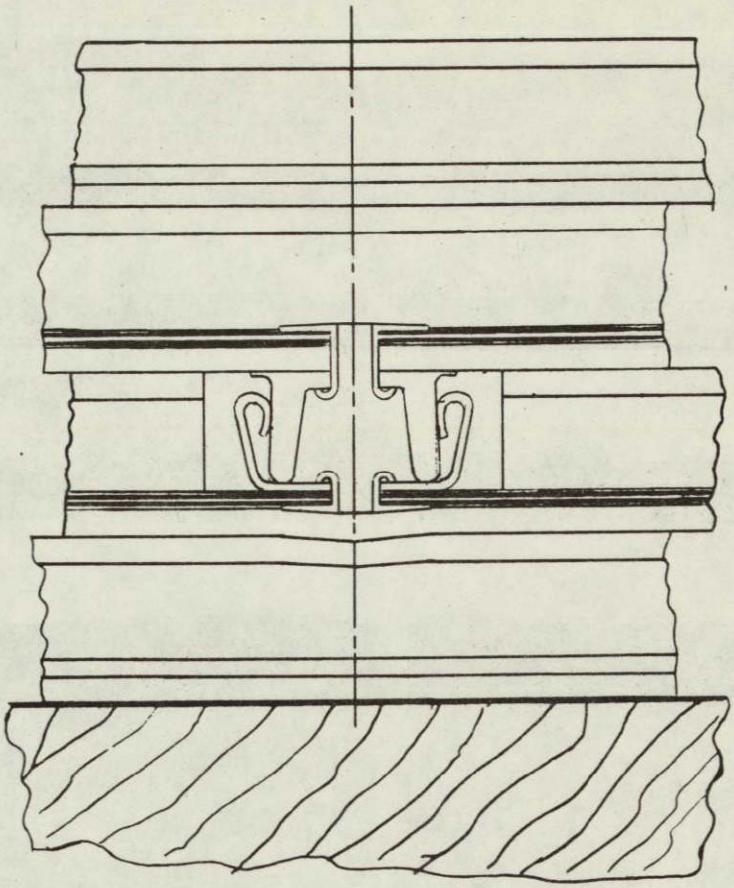

Figure 3-20. Battery Snap Fastener Module Interconnector

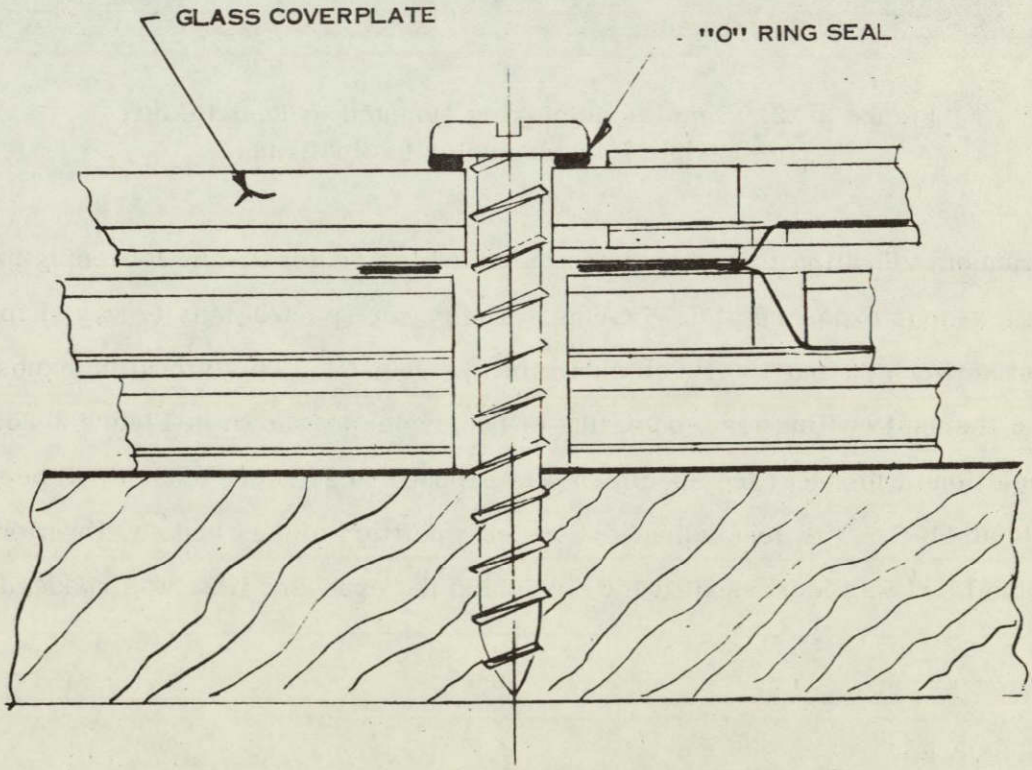

Figure 3-21. Sheet Metal Screw Module Interconnector

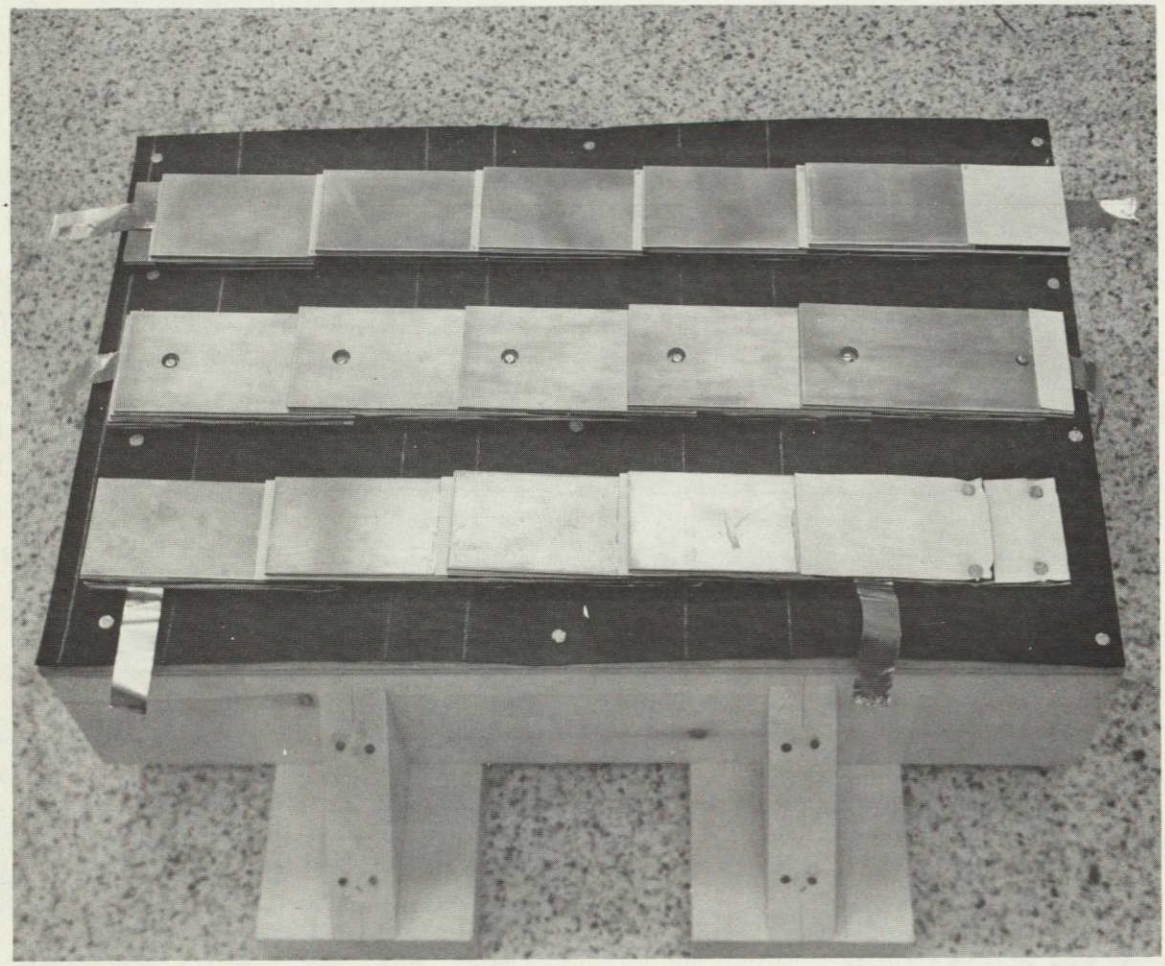

Figure 3-22. Simulated Shingles Mounted to Test Fixture for Module Interconnector Evaluations

The initial random vibration test, which was intended to accelerate any loosening processes, consisted of a 2-hour exposure at 0.75 Grms. The power spectra density was shaped to provide input between 20 and 100 Hz as shown in Figure 3-24. This vibration exposure was followed by a thermal cycling test consisting of two cycles as shown in Figure 3-25. Following the completion of this test the specimen was exposed to 24 hours at 90 to 95 percent relative humidity at 41°C. The concluding test was a repetition of the random vibration test except that the level was increased to 1.0 Grms and the exposure time was reduced to one hour.

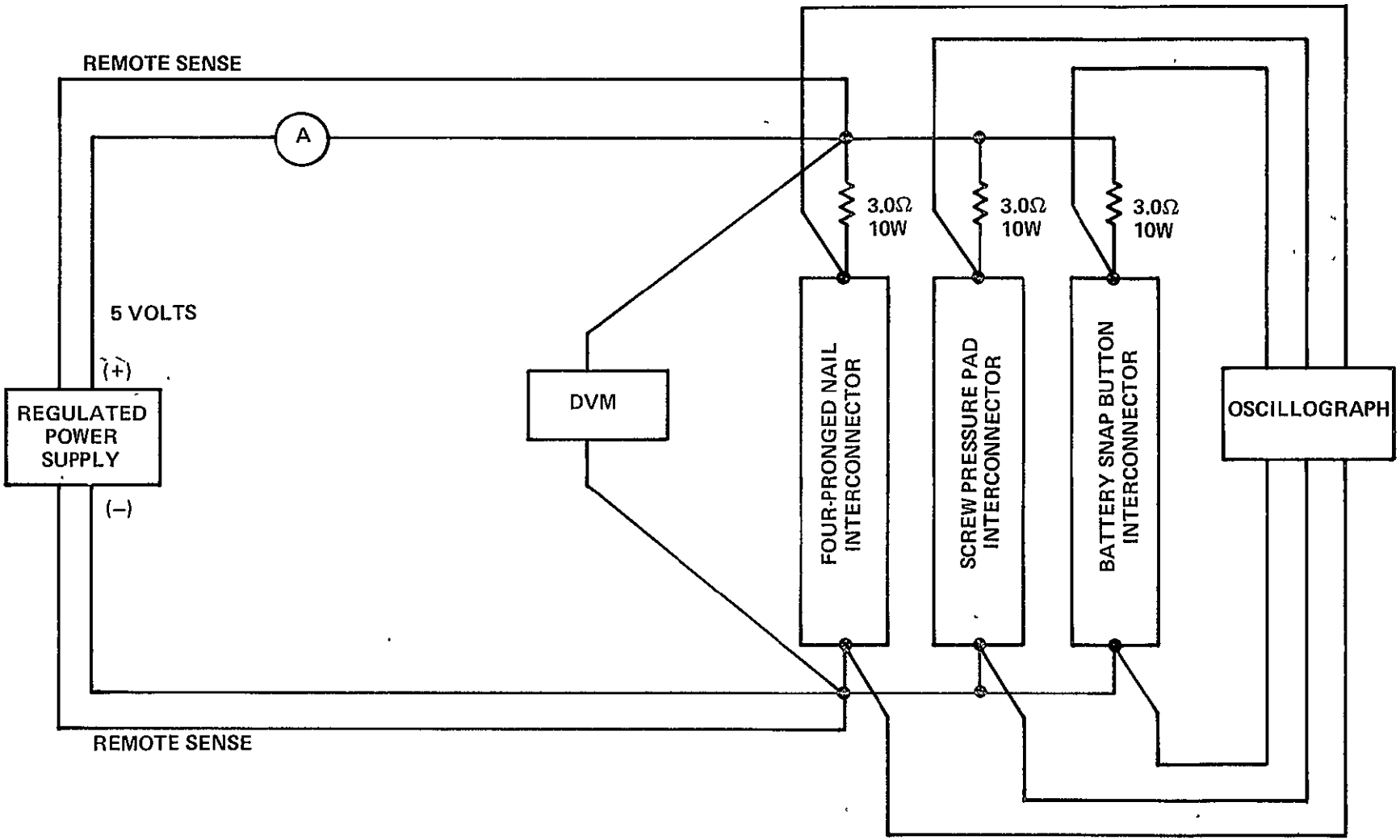

Figure 3-23. Module Interconnection Evaluation - Electrical Schematic

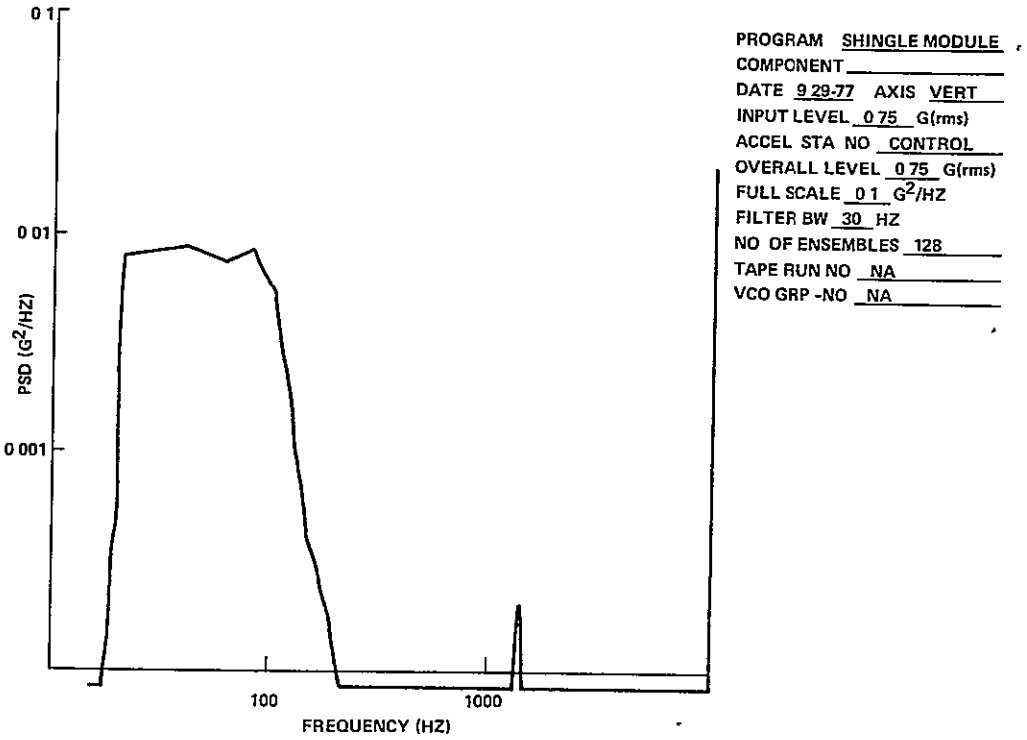

Figure 3-24. Power Spectra Density Plot of Random Vibration Input

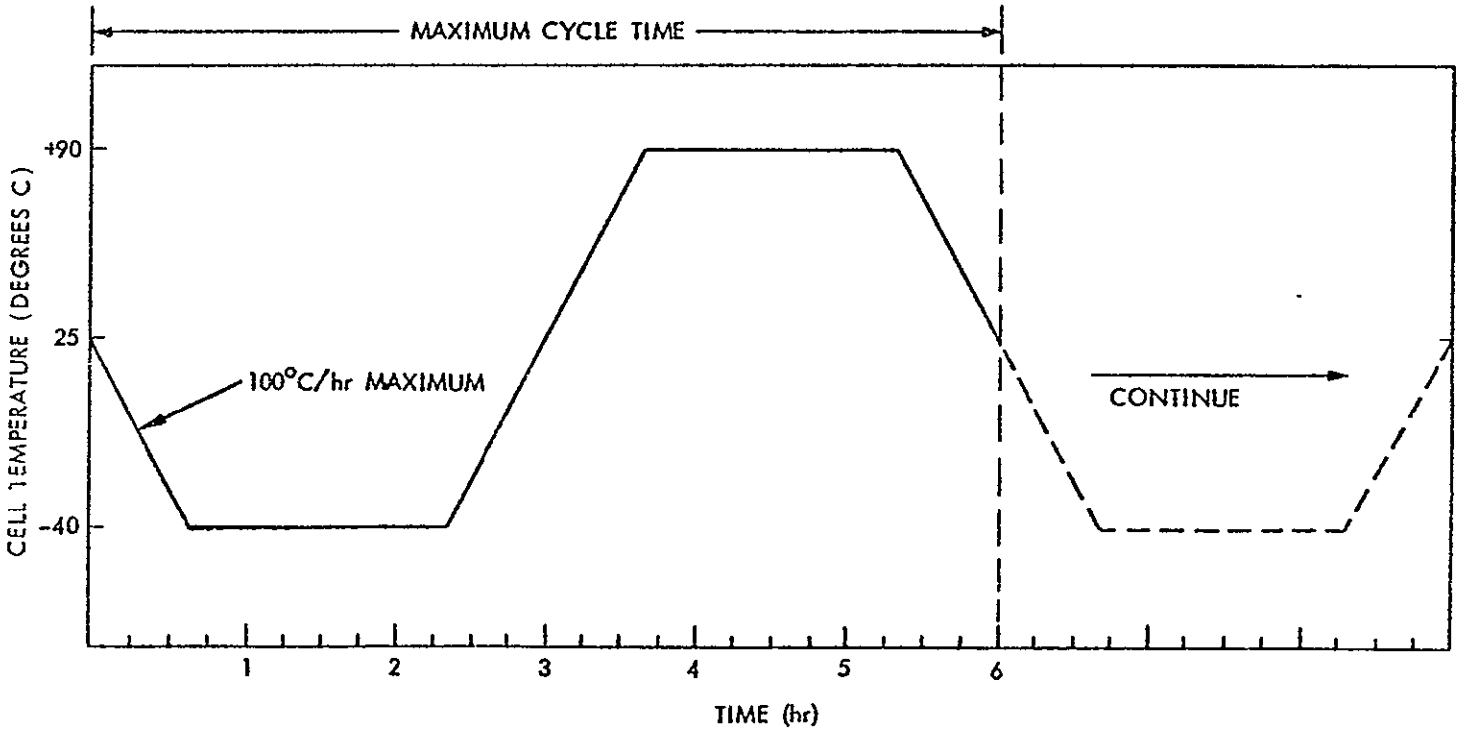

Figure 3-25. Thermal Cycle Test (Shorter cycle time is acceptable if 100°C/hr maximum rate of temperature change is not exceeded.)

The total series resistance of each circuit was monitored throughout this testing sequence with the results as summarized in Table 3-4 for various times during the sequence. The four-pronged nail interconnectors were not installed until after the first random vibration exposure. The battery snap buttons experienced a significant amount of electrical noise during the initial few minutes of the random vibration exposure but this disappeared as the test continued. Following this initial random vibration test the test specimen was exposed to ambient laboratory conditions in the unpowered state for a few days before the start of the thermal cycling test. During this time there was an apparent increase in the series resistance of both the screw pressure pad and the battery snap button interconnectors. In addition the latter interconnectors were again found to be electrically noisy when power was applied at the start of the thermal cycling test. During these two thermal cycles the battery snap button connector circuit was extremely erratic in series resistance with a complete open circuit at one point in the sequence. The 24 hour humidity exposure, which immediately followed the thermal cycling test, resulted in a substantial increase in series resistance for both the four-pronged nail and for the screw pressure pad circuits and a complete open-circuit for the battery snap buttons. This open-circuited condition was permanent from this time through the subsequent final random vibration exposure. This final vibration tests resulted in an improvement for the other two circuits.

A post-test examination of the battery snap buttons revealed that three of the five pairs of buttons were not making electrical contact. Continuity was restored by separating these pairs and deforming the spring clips of the female part to increase the contact force.

A review of these data indicates the significance of the brief humidity exposure on the series resistance of the interconnector joints, probably as a result of the formation of a tarnish film on the contacting copper surfaces in the cases of the screw pressure pad and four-pronged nail configurations, and on the nickel surface in the case of the battery snap button. A survey

Table 3-4. Interconnector Evaluation Test Results

Interconnector Configuration	Number of Interconnector Joints	Total Series Resistance (mΩ)									
		Start-of-Random Vibration Exposure (0 75 Grms)	End-of-Random Vibration Exposure (0 75 Grms)	Thermal Cycling Test						End-of-Humidity Exposure	After Completion of Final Random Vibration Exposure (1 0 Grms)
				T = 25°C	T = -40°C	T = 90°C	T = -40°C	T = 90°C	T = 25°C		
Four-Pronged Nail	5	(1)	(1)	45	45	42	60	54	45	105	54
Screw Pressure Pad	6	52	60	100	106	53	53	58	53	172	150
Battery Snap Buttons	5	87-199	87	175-355	675	169	(2)	425	525	(2)	(2)

(1) Four-pronged nail interconnectors were not installed for the initial random vibration

(2) Open-Circuit

of the literature pertaining to the formation of tarnish films on contacts (References 1, 2 and 3) reveals that significant increases in contact resistance should be expected with either copper or nickel surfaces when exposed to a humid environment particularly in the presence of contaminants such as SO_2, NO_2, and Cl_2. Figures 3-26 and 3-27 which are reproduced from Reference 2, show the effects of various contaminants on the tarnish kinetics and contact resistance for copper. Figure 3-28, which is also from Reference 2, shows that nickel contacts are quickly covered with non-conductive films when exposed to an industrial environment consisting of the following constituents:

H_2S	200 pub
SO_2	200 ppb
NO_2	200 ppb
Cl_2	50 ppb
H_2O	90 percent R. H.

Reference 3 also reports a lack of conductivity for nickel contacts when exposed for 175 hours to a humid environment obtained with water and 8 percent phenol-formaldehyde.

In view of these results and the desire to achieve low contact resistance without the use of costly gold plating, it was decided to implement an interconnection scheme which is modeled after the concept reported in Reference 4. With this approach tin alloy plated non-noble metal contacts are configured as sharp wedges which bear against a mating smooth plated surface. In this manner it is possible to achieve a gas-tight, high-pressure contact. Figure 3-29 shows an adaptation of this concept to the methyl methacrylate module substrate design. The negative terminal in the top substrate layer consists of a solder-plated copper

1. Mano, K., "Studies of Environmental Test Methods of Electrical Contact in Japan", Proceedings of the Holm Seminar on Electrical Contact Phenomena - 1973.

2. Abbott, W. H., "Effects on Industrial Air Pollutants on Electrical Contact Materials", Proceedings of the Holm Seminar on Electrical Contact Phenomena - 1973.

3. Peytchev, L., et. al., "Influence of Aggressive Factors on Some Contact Materials", Proceedings of the Holm Seminar on Electrical Contact Phenomena - 1973.

4. Garte, SM, and Diehl, R. P., "The Successful Utilization of Dry Circuit Base Metal Contacts", paper presented at the 9th Annual Connector Symposium, October 21, 1976.

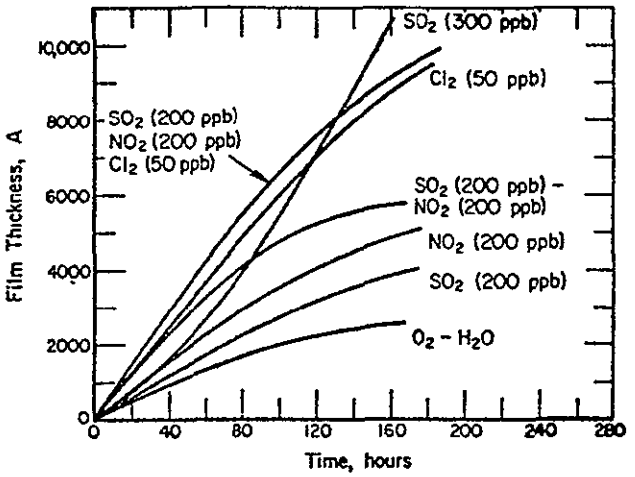

Figure 3-26. Tarnish Kinetics of Copper in N_2-O_2-H_2S (200 ppb) Mixtures with SO_2, NO_2, Cl_2 at 30 C

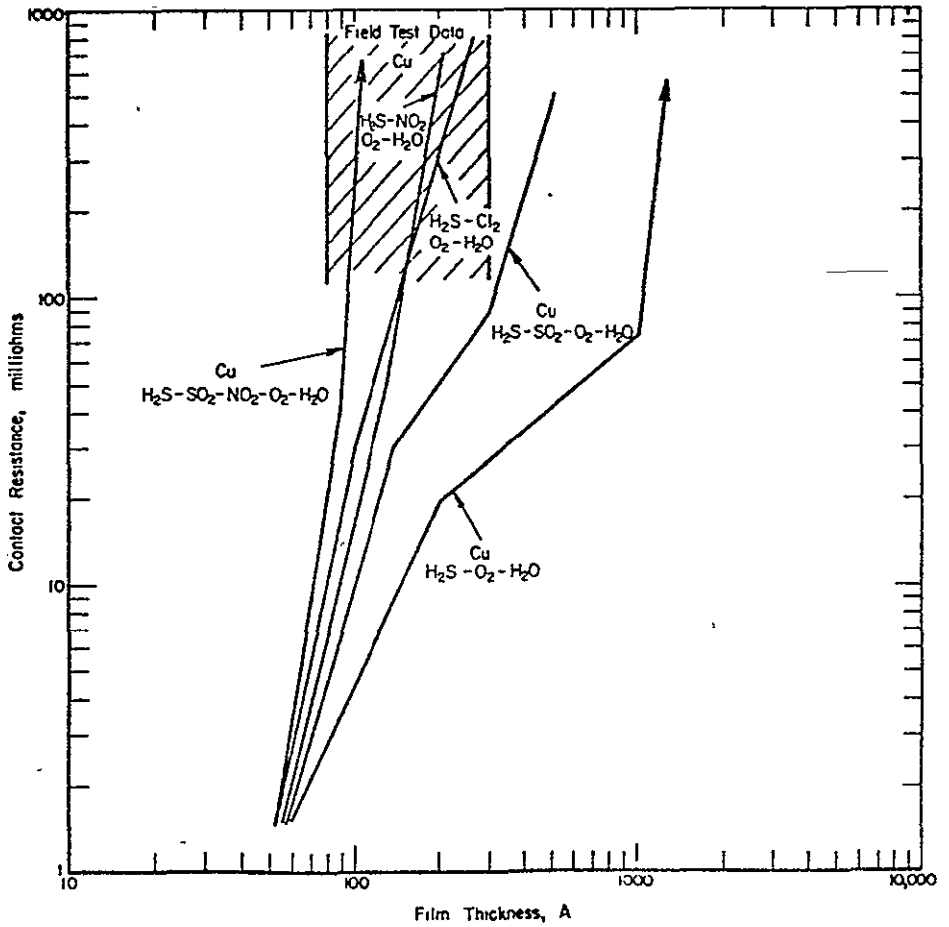

Figure 3-27. Contact Resistance for Copper Versus Film Thickness

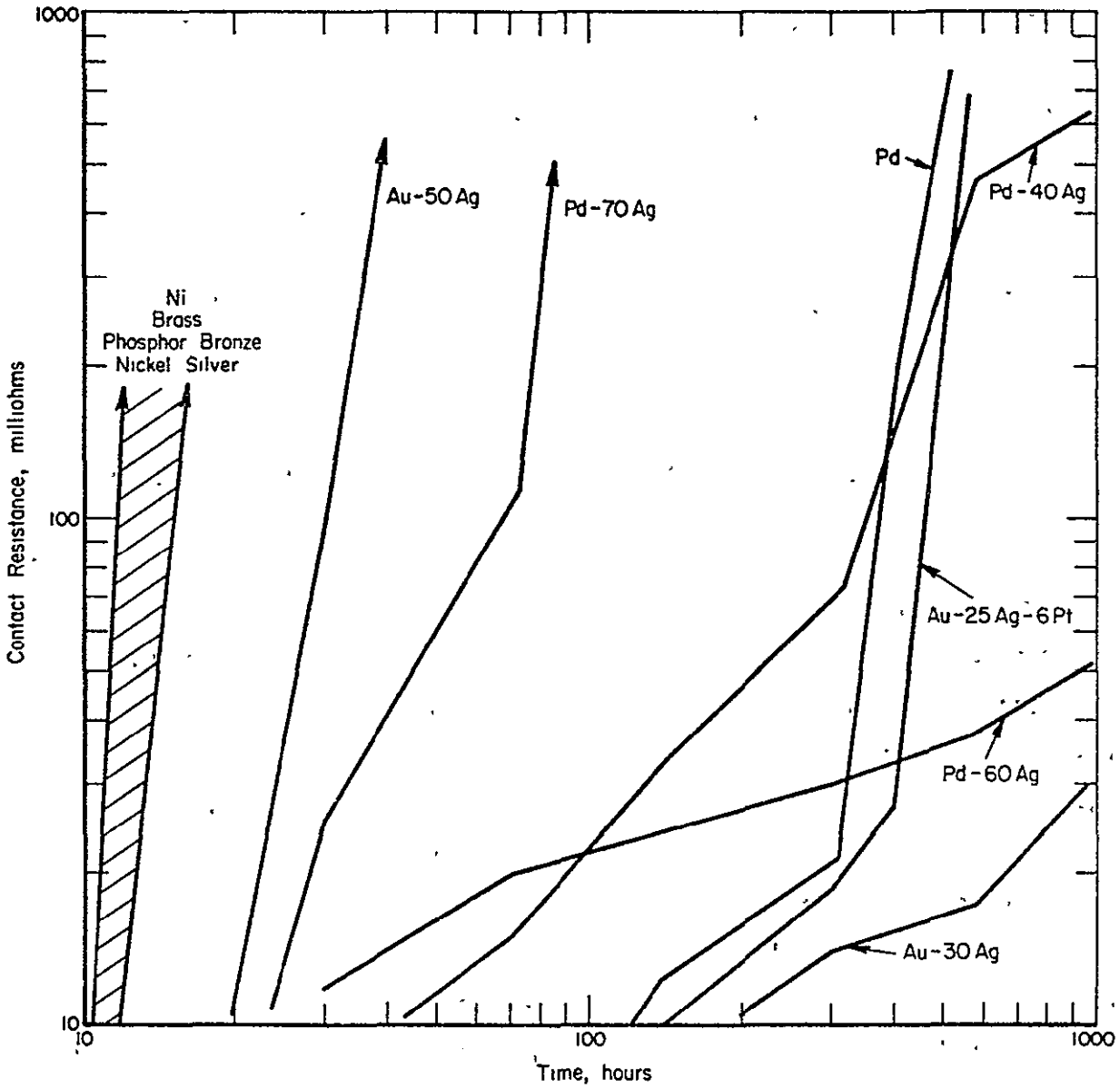

Figure 3-28. Contact Resistance in N_2-O_2-H_2S-SO_2-NO_2-Cl_2-H_2O at 30 C

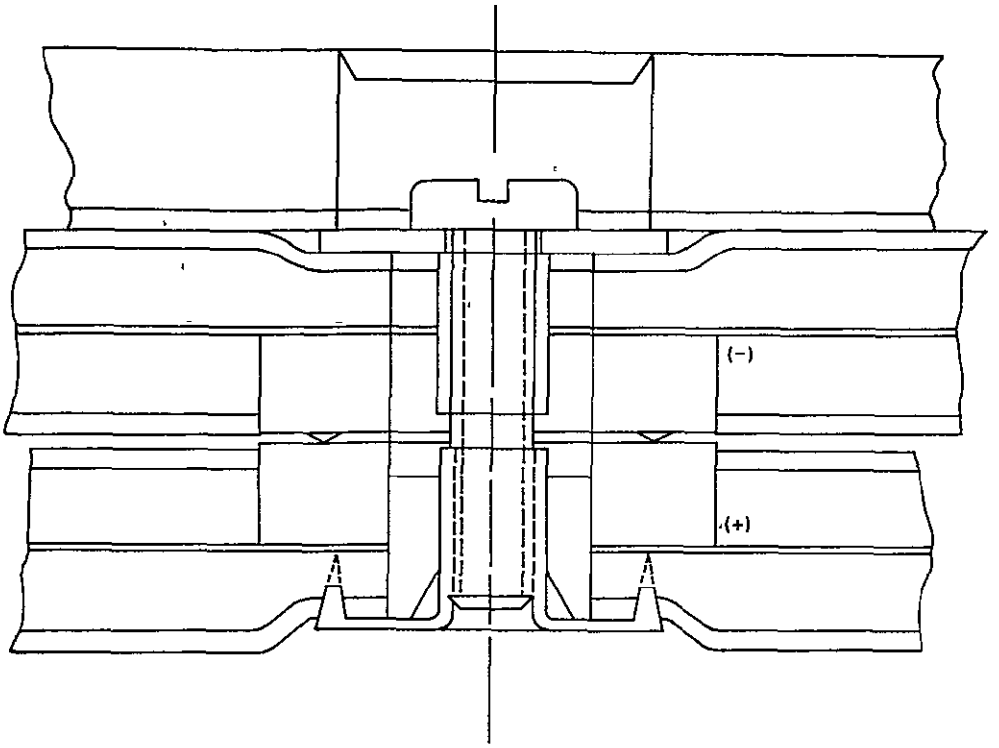

Figure 3-29. Recommended Module Interconnector for MMA Module Design

boss which is provided with three conical projections which bear against the smooth surface of the solder-plated copper boss on the positive terminal of the bottom substrate layer. Clamping pressure between these two layers is provided by a 6-32 machine screw which mates with a captive *TEENUT* in the bottom layer. A 14.3 mm (0.563 inch) diameter washer under the screw head distributes the clamping load over the substrate area. The deflection of the substrate under this washer and under the *TEENUT* flange provides the preload necessary to effect a low resistance contact. A test specimen, shown in Figure 3-30, was prepared to represent this interconnect concept. The upper and lower layers of substrate were joined together with the machine screw as shown in the photograph. This screw was tightened to provide about 1.3 mm (0.05 inch) of deflection of the washer into the top substrate skin. Under this condition the substrate bearing load-deflection curve (see Figure 3-4) indicates a preload of approximately 31 N (7 lb_f) in the contact joint. This is equally distributed among the three conical projections to provide 10.3 N (2.3 lb_f) of contact force. Data from Reference 4 indicate this is adequate force to provide a reliable high-pressure,

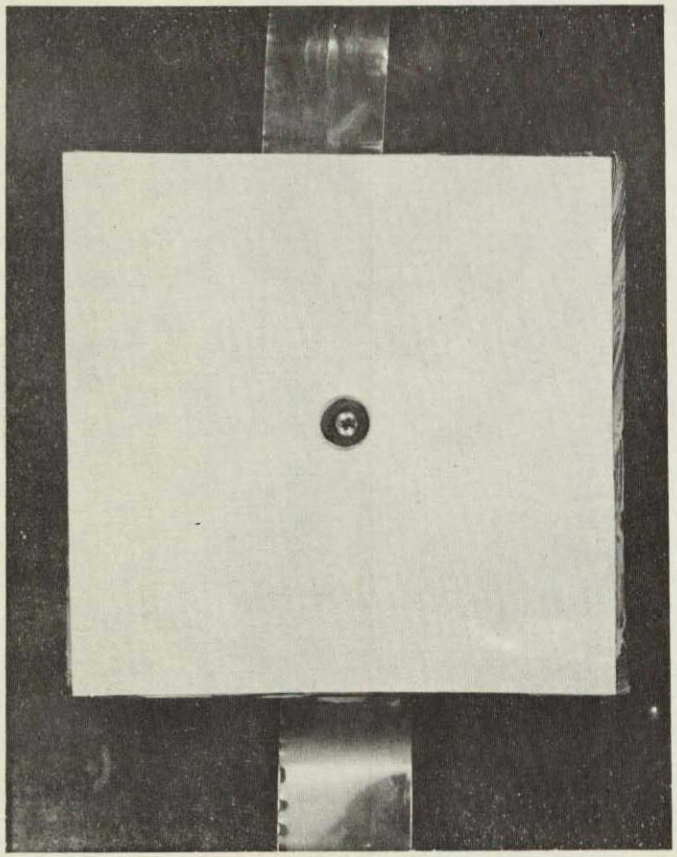

(a) Top Layer

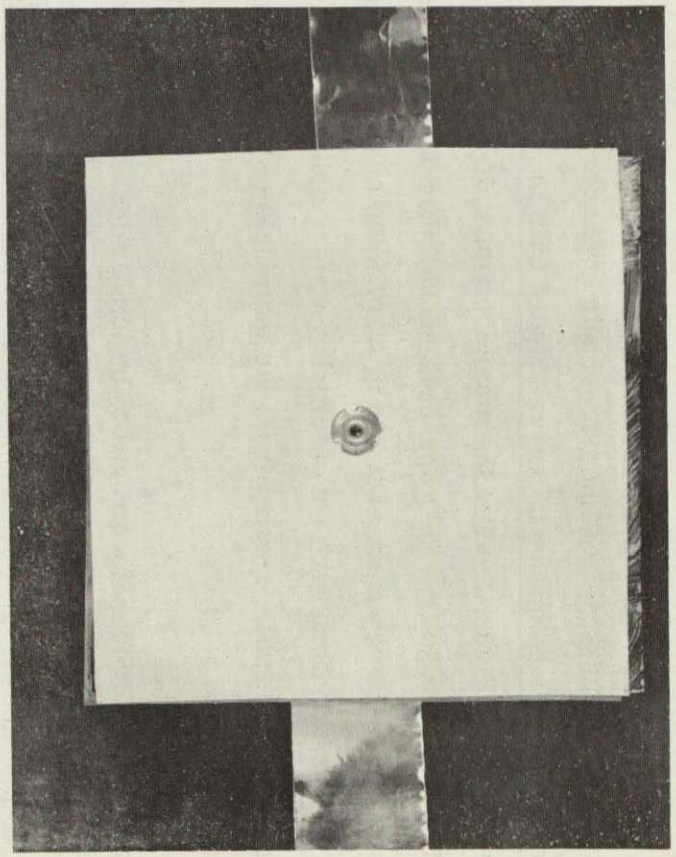

(b) Bottom Layer

Figure 3-30. Test Specimen for Recommended Module Interconnector for MMA Module Design

gas-tight contact. This test specimen was subjected to 20 thermal cycles from -40 to 90° C. The contact resistance of this specimen increased from 1.03 to 1.20 mΩ as a result of this exposure.

Based on the limited testing performed as part of this task activity and on a survey of the literature pertaining to this technology, it is concluded that the interconnector contact configuration represented by Figure 3-29 is the most promising design solution for immediate application on the shingle module. This approach should provide a reliable low-resistance contact which accommodates as much as 1.8 mm (0.07 inch) of misregistration in the overlapping shingle layers. The machine screw which applies the clamping force between the contacting bosses is electrically isolated from the terminals of the module by two insulating sleeves as shown in Figure 3-29.

The four-pronged nail interconnector proved to be impractical from the standpoint of removability for module replacement. The barbs on the pronges hold effectively in the plywood roof sheathing but also prevent the extraction of the nail through the fabric reinforced *FLEXSEAL* substrate skins. The battery snap buttons are a potentially attractive interconnector concept, but it is apparent from this evaluation program that the materials would require change to make this connector survive the environmental constraints of this program. Unfortunately a development effort of this magnitude, which should involve the manufacturer of such connectors, is beyond the scope of this program both in financial resources and in time.

SECTION 4

CONCLUSIONS

SECTION 4

CONCLUSIONS

The selected shingle module design is capable of supplying a maximum power output in excess of 97 Watts/m^2 of module area at 1 kW/m^2 insolation and 60° C operating temperature. This module is particularly suited for mounting to plywood roof sheathing as a direct substitution for conventional asphalt shingles. The dead weight of the shingle modules amounts to 19.7 kg/m^2 (4.0 lb/ft^2), which is slightly greater than the best grade of asphalt shingles.

A typical residential roof installation, which produces a nominal 8 kW peak output at 1kW/m^2 insolation and 60° C, would consist of 1624 modules electrically arranged in a matrix of 28 parallel by 58 series. The series direction (along the sloping height of the roof) could be divided into two electrical sections so that the peak power voltage would be 223 Volts at the nominal conditions stated above. This arrangement of shingle modules would occupy a roof area which is 11.81 m (38.75 ft) from gable-to-gable and 7.20 m (23.62 ft) from eave-to-ridge for a total area of 85.032 m^2 (915.28 ft^2). Thus the overall packing factor for this roof installation, which is defined as the ratio of the nominal solar cell area to the total roof area, is 0.801 and the overall installed areal specific power is 94 watts/m^2 of roof area. This overall installed power density compares favorably with conventional rigid module constructions which use rectangular or hexagonal solar cells.

SECTION 5

RECOMMENDATIONS

SECTION 5

RECOMMENDATIONS

The tempered glass covered module design described in Section 3.1 is recommended as the preferred approach for implementation under Task 5. This design employs embossed glass (ASG *SUNADEX*) as the coverplate material. As recently reported under the New Technology provisions of this contract, this recommended module construction approach will exhibit an enhanced output power as a result of the trapped reflected light from the white interstitial spaces. While the discovery of this phenomena resulted from this contract work, no further attempts have been made to answer some fundamental questions concerning the further application of this enhancement in module output. These questions might include:

1. What is the optimum solar cell packing factor for a given module design and solar cell cost?
2. What is the optimum embossing pattern on the glass coverplate?
3. Would a low solar absorptance coating on the embossed surface in the interstitial spaces improve the enhancement in solar cell output?
4. What properties should the front surface of the coverplate have for optimum performance?

It is recommended that this phenomena be investigated further to more fully understand the enhancement mechanisms and to answer these questions concerning its application to module design.

The use of methyl methacrylate (MMA) as the sole solar cell encapsulant is not practical due to the thermal induced strains resulting from the temperature cycling extremes of -40 and 90°C. The relatively high modulus MMA can not elastically accommodate these strains at the specified low temperature extreme. Fracture of both the MMA casting and the solar cell resulted in all specimens tested. Attempts to buffer coat the solar cells with RTV 615 prior to embedding within MMA have also proved unsuccessful due to a reaction between these two materials which turned the RTV 615 cloudy. The volumetric expansion of the RTV 615 also caused bulges in the MMA casting during high temperature excursions.

The formulation of a lower modulus copolymer with MMA is probably the only method available to accommodate these strains without the other problems associated with buffer coating. It is recommended that this approach be further investigated as part of the on-going effort under Task 3 of the LSSA Project.

SECTION 6

NEW TECHNOLOGY

SECTION 6

NEW TECHNOLOGY

On November 14, 1977 a New Technology disclosure entitled "A Zero Depth Solar Photovoltaic Concentrator", was submitted by N. F. Shepard, Jr. This disclosure describes a zero depth concentrator for planar solar cell modules which employs embossed glass (e. g., ASG *SUNADEX*) to trap, by repeated internal reflection, the light incident on white interstitial spaces to effectively concentrate this otherwise wasted flux onto the active solar cell surface where it can be converted by the photovoltaic process into enhanced electrical output. Figure 3-13 shows the effect of this phenomena on module electrical output as a function of the overall solar cell packing factor.

GENERAL ELECTRIC

Space Division

Headquarters Valley Forge, Pennsylvania ☐ Daytona Beach, Fla ☐ Evendale, Ohio

☐ Huntsville, Ala ☐ Bay St Louis, Miss. ☐ Houston, Texas ☐ Sunnyvale, Calif.

☐ Beltsville, Md ☐ Tacoma, Wash ☐ Palmdale, Calif ☐ Bedford, Mass.

☐ Washington, D C Area